BANGMOD INTERNATIONAL JOURNAL OF MATHEMATICAL & COMPUTATIONAL SCIENCE
ISSN: 2408-154X
https://bangmodjmcs.com/
Volume 8 (2022)
Pages 65–99

SEMI-ANALYTICAL INVESTIGATION ON MHD OLDROYD-B NANOFLUID FLOW UNDER STRATIFICATION CONDITIONS VIA AN EXPONENTIALLY STRETCHING SURFACE

Auwalu Hamisu Usman [1,2], **Zahir Shah**[3], **Waris Khan**[4], **Usa Wannasingha Humphries** [1*]
[1] *Department of Mathematics, Faculty of Science, King Mongkut's University of Technology Thonburi, 126 Pracha Uthit Road, Bang Mod, Thung Khru, Bangkok 10140, Thailand.*
E-mails: usa.wan@kmutt.ac.th
[2] *Department of Mathematical Sciences, Faculty of Physical Sciences, Bayero University, Kano, Nigeria.*
E-mails: ahusman.mth@buk.edu.ng
[3] *Department of Mathematics, University of Lakki Marwat, Lakki Marwat, Pakistan*
E-mails: zahir1987@yahoo.com
[4] *Department of Mathematics and Statistics, Hazara University Mansehra, Khyber Pakhtunkhwa, Pakistan*
E-mails: wariskhan758@yahoo.com

**Corresponding author.*

Received: 1 November 2022 / Accepted: 25 December 2022

Abstract In this paper, a semi-analytical method is used to investigate the effects of stratification conditions on the boundary layer MHD Oldroyd-B nanofluid flow passed through an exponentially stretching sheet. Thermal radiation, viscous dissipation, as well as thermophoretic velocity effects are taken into account. Microorganism theory is also considered to analyze the suspended nanoparticles through bioconvection. The consequences of several features regarding Heat and mass transfer have been addressed. Using suitable transformations, the dimensionless equations obtained and solved by homotopy analysis method (HAM). The behavior of all profiles is described graphically and numerically by using an appro-

Published online: 31 December 2022

Please cite this article as: A.H. Usman et al., Semi-analytical investigation on mhd oldroyd-b nanofluid flow under stratification conditions via an exponentially stretching surface, Bangmod J-MCS., Vol. 8 (2022) 65–99.

https://doi.org/10.58715/bangmodjmcs.2022.8.6
Bangmod J-MCS 2022

priate set of input parameters. With increasing thermal stratification parameter and Deborah numbers with respect to the relaxation time of heat flux, the Nusselt number increases and decreases respectively. Mass flux decrease by increasing the concentration stratification parameter. The comparison with existing literature reveals a high level of agreement.

MSC: 76B70

Keywords: Bioconvection, Exponentially stretching sheet, Oldroyd-B nanofluid, stratification conditions, thermal radiation, thermophoretic

1. Introduction

The viscosity law of Newton is violated by the majority of working fluids in engineering and industrial mechanisms. Such fluids are known as non-Newtonian fluids. Toothpastes, blood with low shear rates, salad cream, paper pulp, polymer solutions, chocolate pudding, paints are examples of such fluids as stated by Irgens [1]. A well-known Navier-Stokes theory fails to sufficiently explain the non-Newtonian materials properties, detail can be seen in Chhabra [2]. Many existing models for analyzing the behavior of non-Newtonian fluids were proposed by considering one of the three types of models: integral, differential, and rate [3–6]. One type of these non-Newtonian fluids that exhibits both relaxation and retardation are called Oldroyd-B fluids proposed by Oldroyd [7]. Unlike other polymeric materials, the typical relationship between shear rate and shear stress in an easy shear flow cannot adequately describethe Oldroyd-B fluids. However, in the past few years, the Oldroyd-B fluid has gained considerable attention among several fluids of rate type, as it includes the classical Newtonian fluid and the Maxwell fluid as special cases. Due to the credibility of its applications, extensive research on the Oldroyd-B fluid flow has been conducted and is still ongoing. Lu et al. [8] studied the influence of nonlinear thermal radiation and homogeneousheterogeneous reaction on three-dimensional MHD Oldroyd-B fluid flow. Zhang et al. [9] investigated on the unsteady double diffusion Cattaneo-Christov Oldroyd-B fluid thin film flow with viscous dissipation and chemical reaction effects. Tlili et al. [10] proposed a mathematical model for the Oldroyd-B nanofluid over a stretching cylinder with activation energy and second order slip in bioconvection. Some studies can be found in the references [11, 12].

In heat transfer, conventional fluids with low thermal conductivities, such as oil, water, and ethylene glycol, cannot solve cooling rate problems. Addition of ultrafine nanoparticles to conventional fluids can improve their thermal conductivities. As a result, nanofluids have been demonstrated to be the primary source for increasing the thermal conductivity of conventional fluids. Because of their intriguing properties, nanofluids are useful in a wide range of technological and engineering applications. Choi and Eastman [13] were the first to coined the term nanofluid and demonstrated how adding nanoparticles to conventional fluids improved their thermal conductivity properties. Buongiorno [14] introduced a model that incorporates Brownian motion and thermophoresis mechanisms to evaluates the consensuses of thermal conductivity of nanofluids. Kumar et al. [15] studied the in-

 https://doi.org/10.58715/bangmodjmcs.2022.8.6

fluence of viscous dissipation and joule heating characteristics of an Oldroyd-B nanofluid flow in three dimensions with thermal radiation effects. Irfan et al. [16] investigated on the flow of an Oldroyd-B nanofluid with variable thermal conductivity and implement thermal and solutal stratifications conditions. Khan et al. [17] considered using motile organisms to study bioconvection flow in an Oldroyd-B nanofluid and an efficient Prandtl method. Some studies on nanofluids flow are included in the references [18–20, 22].

There are substantial body literature on the fluid flow through a stretching sheet with a velocity (linear) proportional to the difference from the set roots. Furthermore, it has been clearly demonstrated that realistically stretching a plastic sheet is not always linear. Sajid and Hayat [23] analyzed the flow induced by an exponentially stretching surface with thermal radiation effects. Gireesha et al. [24] make use of Saffman flow model to explore on the dusty fluid flow with heat transfer through an exponentially stretching surface considering the role of a magnetic field. Shafiq et al. [25] used a statistical approach to investigate the mixed convective boundary layer third-grade fluid flow through an exponentially stretching surface. Nadeem et al. [26] investigated on the transportation of slip influence on micropolar nanofluid flow over an exponentially stretching surface.

Stratification is a natural occurrence of layer formation caused by temperature variations, varying fluids densities, and concentration differences. Physically, there is great interest in investigating the effects of thermally and solutely stratifications on the convective flow of nanofluids. However, stratification also occurs in waterways, lakes, thermal storage systems, oceans, and surface reservoirs. Cheng [27] investigated on the natural convection fluid flow with implementation of mass and thermal stratifications over a saturated porous vertically wavy surface using power-law. Koriko et al. [28] investigated the effects of radiation and stratification conditions on micropolar fluid flow along a vertical surface. Daniel et al. [29] studied the stratified convective MHD nanofluid flow. Tlili et al. [30] examined an analytical solution for 3D Maxwell nanofluid flow considering the effects of radiation and chemical reactions under double stratification conditions. Mallawi et al. [31] investigated the effects of radiation and double-stratification on non-Newtonian liquid convective flow with Cattaneo-Christov double-flux in a Riga plate. Under stratification, Waqas et al. [32] studied the effect of thermo-solutal Robin conditions in thermally radiative MHD nanofluids flow.

The term bioconvection refers to pattern-forming macroscopic convective particles movements formed in the suspension of swimming microorganisms as a result of variations in the density gradient. The swimming of collective motile microorganisms changes the density of the base fluids, which affects macroscopic particles motion. When compared to motile microorganisms, nanoparticles are not self-driven, and their movement is caused by Brownian motion and the thermophoresis effect. Bioconvection in nanofluids is expected to be possible withlow nanoparticle concentration, but it will not be capable of providing a significant increase in base fluid viscosity. Bhatti and Michaelides [33] investigated thermo-bioconvection nanofluid flow with activation energy effects through a Riga plate. Farooq et al. [34] investigate the thermally radioactive Carreau nanofluid flow using modified Cattaneo-Christov model and exponentially spatial heat source. Waqas et al. [35] investigated the Oldroyd-B nanofluid flow through a rotating disk using numerical simulations with bioconvection and nonlinear radiation. Awais et al. [36] uses a numerical approach to investigate mass and heat transfer and the effects of variable conductivities on MHD nanofluid flow rheology with bioconvective theory. Khan et al. [37] studied the

https://doi.org/10.58715/bangmodjmcs.2022.8.6
TaCS Publications
Bangmod J-MCS 2022

effects of bioconvection and partial slip on the Oldroyd-B nanofluid flow induced by a convectively heated surface.

Furthermore, no attempts have been made to date, to the best of the author's knowledge, to explore the free convective boundary layer flow of three-dimensional Oldroyd-B nanofluid over an exponentially stretching sheet with the application of stratification conditions and bioconvection. The goal of this paper is to use a semi-analytical approach to investigate the effects of stratification conditions on the Oldroyd-B nanofluid flow and heat transfer characteristics through an exponentially stretching sheet. The suspended nanoparticles caused by bioconvection are analyzed using microorganism theory. The influences of thermophoretic, radiation, viscous dissipation, and chemical reactions are considered. The homotopy analysis method (HAM) used to obtained the solutions. Initially, Liao [38–40] demonstrated this method which does have a quick convergent solutions and several advantages over other existing methods. Because of its fast convergence, it has piqued the interest of a number of researchers in this field, like used in the references [41–45].The obtained results with all related parameters across all the profiles are depicted graphically. An important component of the developed model is the verification of the results obtained through the correlation of the previously published material in the literature. Prestigious consistency has indeed been achieved in this regard.

2. Formulation of the Problem

Consider the steady, incompressible, three-dimensional Oldroyd-B nanofluid flow with bioconvection and stratification conditions through an exponentially stretching surface. The flow is bounded by $z \geqslant 0$. Moreover, the effects of viscous dissipation, thermal radiation, heat suction/injection, chemical reaction, and thermophoretic velocity on the heat and mass transfer characteristics are also taken into account. The fluid is electrically conducted along the z-axis in the presence of a uniform magnetic field of strength B_0 is applied in the z-direction and with the assumption that the Reynolds number is very small in order to ignore the induced magnetic field effect. Let $u_w = U_{ref} e^{(\frac{x+y}{l})}$ be the fluid velocity in the x direction and $v_w = V_{ref} e^{(\frac{x+y}{l})}$ be the fluid velocity in y direction along the sheet. Taking ambient temperature T_∞, ambient concentration C_∞, ambient density of microorganisms N_∞, see the geometry of the problem in Figure 1.
The constitutive equations of Oldroyd-B fluid model [8] are given by

$$div\mathbf{V} = 0, \tag{2.1}$$

$$\rho \frac{d\mathbf{V}}{dt} = div\mathbf{V} \tag{2.2}$$

Here, the Cauchy stress tensor $\mathbf{T}$ and extra stress tensor $\mathbf{S}$ are given as

$$\mathbf{T} = -\rho\mathbf{I} + \mathbf{S}, \tag{2.3}$$

$$\mathbf{S} = \alpha_1 \frac{D\mathbf{S}}{Dt} = \mu \left(A_1 + \alpha_2 \frac{DA_1}{Dt} \right), \tag{2.4}$$

with $\frac{D}{Dt}$ as the covariant differentiation and α_1 and α_2 respectively as fluid relaxation and retardation time. The first Rivilin-Ericksen tensor A_1 is defined as

$$A_1 = grad\mathbf{V} + (grad\mathbf{V})^T, \tag{2.5}$$

https://doi.org/10.58715/bangmodjmcs.2022.8.6

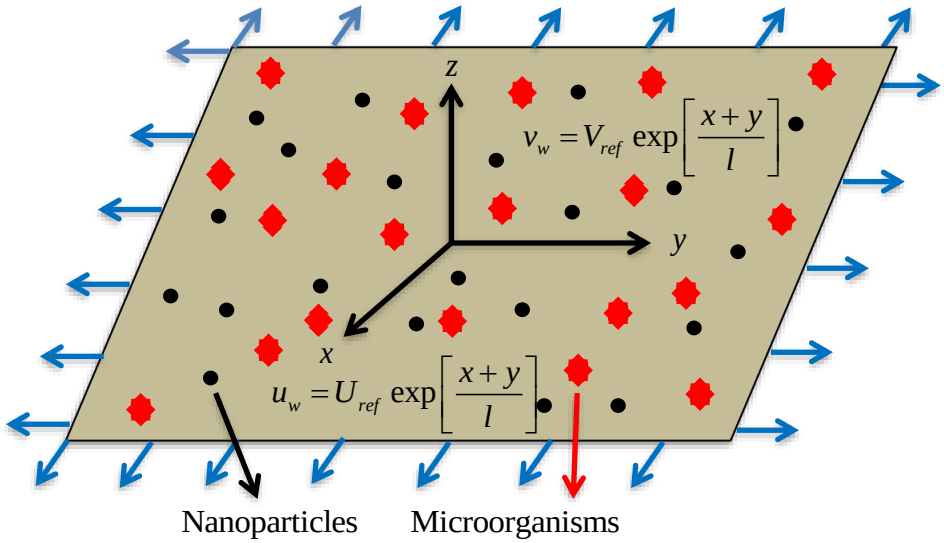

FIGURE 1. Schematic diagram of the problem.

where T is the transpose of a matrix and the velocity field $\mathbf{V}$ is represented by

$$\mathbf{V} = [u(x,y,z), v(x,y,z), w(x,y,z)]\,. \tag{2.6}$$

The derivative $\frac{D}{Dt}$ is given

$$\frac{Da_i}{Dt} = \frac{\partial a_i}{\partial t} + u_r a_{i,r} - u_{i,r} a_r. \tag{2.7}$$

The energy equation in the vector form are defined as

$$\rho C_p(\mathbf{V}.\nabla\mathbf{T}) = \nabla.q - \nabla q_r + Q^*(T - T_\infty), \tag{2.8}$$

where Q^* is the heat reaction and q is the heat flux and defined by the Cattaneo-Christov model given by

$$q + \alpha_3\left[\frac{\partial q}{\partial t} + \mathbf{V}.\nabla q - q.\nabla + (\nabla.\mathbf{V})q\right] = \nabla(kT), \tag{2.9}$$

where α_3 is the thermal relaxation time, k is the thermal conductivity and T is the temperature. The governing equations [10, 25, 46] are

$$w_z + v_y + u_x = 0, \tag{2.10}$$

$$\begin{aligned} &wu_z + vu_y + uu_x + \alpha_1\left[u^2u_{xx} + v^2u_{yy} + w^2u_{zz} + 2uvu_{xy} + 2uwu_{xz} + 2vwu_{yz}\right] \\ &= \nu_f\left[u_{zz} + \alpha_2\left(uu_{xzz} + vu_{yzz} + wu_{zzz} - u_xu_{zz} - u_zw_{zz} - u_yv_{zz}\right)\right] \\ &+ \frac{\sigma B_0^2}{\rho_f}\left(-u - \alpha_1 wu_z\right), \end{aligned} \tag{2.11}$$

https://doi.org/10.58715/bangmodjmcs.2022.8.6

$$wv_z + vv_y + uu_x + \alpha_1\left[u^2v_{xx} + v^2v_{yy} + w^2v_{zz} + 2uvv_{xy} + 2uwv_{xz} + 2vwv_{yz}\right]$$
$$= \nu_f\left[v_{zz} + \alpha_2\left(uv_{xzz} + vv_{yzz} + wv_{zzz} - v_xw_{zz} - v_zw_{zz} - v_yv_{zz}\right)\right]$$
$$+ \frac{\sigma B_0^2}{\rho_f}\left(-v - \alpha_1 wv_z\right), \tag{2.12}$$

$$wT_z + vT_y + uT_x + \alpha_3\left[w^2T_{zz} + v^2T_{yy} + u^2T_{xx} + 2uvT_{xy} + 2vwT_{yz} + 2uwT_{xz}\right.$$
$$\left. + \left(uu_x + vu_y + w\ u_z\right)T_x + \left(uw_x + vw_y + ww_z\right)T_z + \left(uv_x + vv_y + wv_z\right)T_y\right]$$
$$= \alpha_f T_{zz} + \tau\left[D_BC_zT_z + \frac{D_T}{T_\infty}\left(T_z\right)^2\right] + \frac{16\sigma^*T_\infty^3}{3k^*(\rho c_p)_f}T_{zz} + \frac{Q_1}{(\rho c_p)_f}(T - T_\infty)$$
$$+ \frac{\mu_f}{(\rho c_p)_f}\left[\left(u_z\right)^2 + \left(v_z\right)^2\right], \tag{2.13}$$

$$wC_z + vC_y + uC_x + = D_BC_{zz} + \frac{D_T}{T_\infty}T_{zz} - \left(V_T(C - C_\infty)\right)_z - k_r(C - C_\infty), \tag{2.14}$$

$$wN_z + vN_y + uN_x + \frac{bW_c}{(C_w - C_\infty)}\left(NC_z\right)_z = D_NN_{zz}, \tag{2.15}$$

with initial boundary conditions

$$u = u_w = U_{ref}e^{\left(\frac{x+y}{l}\right)}, u = v_w = V_{ref}e^{\left(\frac{x+y}{l}\right)}, w = 0, T = T_w = T_{ref} + a_1e^{\left(\frac{x+y}{2l}\right)},$$
$$C = C_w = C_{ref} + a_2e^{\left(\frac{x+y}{2l}\right)}, N = N_w = N_{ref} + a_3e^{\left(\frac{x+y}{2l}\right)} \text{at } z = 0, \tag{2.16}$$
$$u \to 0, v \to 0, w = 0, T \to T_\infty = T_{ref} + b_1e^{\left(\frac{x+y}{2l}\right)}, C \to C_\infty = C_{ref} + b_2e^{\left(\frac{x+y}{2l}\right)},$$
$$N \to N_\infty = N_{ref} + b_3e^{\left(\frac{x+y}{2l}\right)} \text{as } z \to \infty \tag{2.17}$$

with (u,v,w) as the velocities on (x,y,z) axes respectively, temperature T, concentration C, gyrotactic microorganism N, wall temperature T_w, wall concentration C_w, wall gyrotactic microorganism N_w, D_B, D_T and D_N are the diffusion coefficient of Brownian motion and thermophoresis and microorganism respectively, α_1, α_2, α_3 are fluid relaxation time, retardation time and thermal relaxation time, τ is heat capacitance ratio, ρ_f is density of the fluid, α_f thermal diffusivity, k_f and σ are thermal and electrical conductivity of the fluid, μ_f is the dynamic viscosity, ν_f kinematic viscosity, Q_1 heat generation/absorption coefficient, B_0 magnetic field, $(\rho c_p)_f$ heat capacitance of the fluid, k_r 1st order chemical reaction dimensional parameter, b chemotaxis, W_c speed of gyrotactic cell.

The thermophoretic velocity of particle colloidal is expressed as

$$V_T = \frac{-k_t}{T_{ref}}\frac{\partial T}{\partial z} \tag{2.18}$$

with the thermophoretic coefficient and temperature reference given by k_t and T_{ref}. The term, $\frac{16\sigma^*T_\infty^3}{3k^*(\rho c_p)_f}\frac{\partial^2T}{\partial z^2}$ and $\frac{Q_1}{(\rho c_p)_f}(T - T_\infty)$ in equation 2.13 are representing the thermal

https://doi.org/10.58715/bangmodjmcs.2022.8.6

radiation term by using the Rosseland approximation for radiation and heat generation/absorption respectively. Using the similarity transformation as in [45]

$$u = U_{ref}e^{\left(\frac{x+y}{l}\right)}f'(\zeta), v = U_{ref}e^{\left(\frac{x+y}{l}\right)}h'(\zeta), w = -\left(\frac{\nu_f U_{ref}}{2l}\right)^{\frac{1}{2}}(f+h+\zeta(f'+h'))e^{\left(\frac{x+y}{2l}\right)},$$
$$T = T_\infty + T_{ref}e^{\left(\frac{x+y}{2l}\right)}\theta(\zeta), C = C_\infty + C_{ref}e^{\left(\frac{x+y}{2l}\right)}\phi(\zeta), N = N_\infty + N_{ref}e^{\left(\frac{x+y}{2l}\right)}\chi(\zeta), \tag{2.19}$$

with f and h are velocities(dimensionless) along x and y axes respectively, θ, ϕ, χ are temperature, concentration and microorganism field (dimensionless) respectively, U_{ref}, V_{ref}, are reference velocities on x and y axes respectively, T_{ref}, C_{ref}, N_{ref} are reference temperature, concentration and microorganism respectively.

$$f''' + ff'' + hf'' - 2h'f' - 2f'^2 - \beta_1\Big[(4+\zeta^2)(f'^3 + h'^2f' + 2h'f'^2)$$
$$+ (5\zeta+\zeta^2)(f'^2f'' + h'^2f'' + h'f'f'') + (f^2f' + 2hff' + 2ff'^2 - 12ff''$$
$$- 12f'f'' - h^2f' - 12hf'') + \zeta(2h'ff' - 4ff''' + 2hf'^2 + 2hh'f' - 4hf''' - 12h'f'')$$
$$+ 4\zeta^2(f'f''' + hf''')\Big] + \beta_2\Big(6f'f''' + 8h'f''' - ff''' - hf''' - 2h'''f' + 3f''^2$$
$$+ 3h''f'' + \zeta(f'f''' + h'f''')\Big) - M^2\big(f' - \beta_1(ff'' + hf'' + \zeta(f'f'' + h'f''))\big) = 0, \tag{2.20}$$

$$h''' - f'h'2h'^2 + fh'' + hh'' - \beta_1\Big[4f'^2h' + hh''' + fh''' + 8fh'^2 + h'^3 - 6fh'h''$$
$$- 6f'hh'' + 6hh'h'''\zeta\big(f'^2h'' - h'^2h'' + h'h''' - f'h''' - 2f'hh''' - 2hh'h''' - 2fh'h'''$$
$$- 2ff'h''' + f'hh''' + 2f'h'h'''\big) + \zeta^2\big(f'^2h''' - h'^2h''' - 4fh'h'''\Big] + \beta_2\Big(8h'''f' + 8h'h'''$$
$$- fh''' - hh''' - 2h'f''' - 2h'f''' + 3h''f'' + 3h''^2\zeta(f'h''' + h'h''')\Big)$$
$$- M^2\big(h' - \beta_1(fh'' + hh'' + \zeta f'h'' + \zeta h'h'')\big) = 0, \tag{2.21}$$

$$\Big(1 + \frac{4}{3}Rd\Big)\theta'' + Pr\big[f\theta' + h\theta' - f'\theta - h'\theta\big] - \beta_3 Pr\Big[3f'^2\theta + 3h'^2\theta - 3h'^2\theta' + 3f'h'\theta$$
$$- f^2\theta'' - 2fh\theta'' - 3h'f\theta' - 3hh'\theta' - 5ff'\theta' - ff''\theta - hf''\theta - fh''\theta - hh''\theta$$
$$- hf'\theta' + 2ff'\theta' + 2hf'\theta + \zeta\big(f'^2\theta'' + 3h'^2\theta' - 4fh'\theta'' - 4hf'\theta'' - 2f'h'\theta'' - fh''\theta'$$
$$+ fh''\theta\big) + \zeta^2\big(f'^2\theta'' - 2h'^2\theta''\big)\Big] + Pr\big[Nb\phi'\theta' + Nt\theta'^2 + Ec(f''^2 + h''^2)\big]$$
$$+ Pr\big[Q\theta - s_1(f' + h')\big] = 0, \tag{2.22}$$

$$\phi'' + Sc(f+h)\phi' - Sc\big[\delta_r\phi' + \tau(\theta'' + \theta'\phi')\big] + \frac{Nt}{Nb}\theta'' - Scs_2(f'+h') = 0, \tag{2.23}$$

https://doi.org/10.58715/bangmodjmcs.2022.8.6

$$\chi''+Sc_b(f+h)\chi'-Sc_b(f'+h')\chi-Pe\left[\phi\chi+(\chi+\delta_n)\phi''\right]-Sc_bs_3(f'+h')=0, \quad (2.24)$$

with the boundary conditions

$$f'(0)=1, f(0)=0, h'(0)=\alpha, \theta(0)=1-s_1, \phi(0)=1-s_2, \chi(0)=1-s_3,$$
$$f'\to 0, h\to 0, \theta\to 0, \phi\to 0, \chi\to 0, as\,\zeta\to\infty, \quad (2.25)$$

with α as velocity ratio parameter, Deborah numbers β_1 in terms of relaxation, β_2 retardation time, and β_3 heat flux relaxation time, M magnetic field parameter, Q is heat generation/absorption parameter(non-dimensional), Rd is the radiation parameter, Pr Prandtl number, Nt thermophoretic parameter, Ec Eckert number, Nb Brownian motion parameter, δ_r reaction parameter, Sc is the Schmidt number, Pe Peclet number, Sc_b Schmidt number of bio-convection, δ_n is the bioconvection constant, s_1, s_2, s_3 are the thermal, concentration, microorganism stratification parameters respectively, quantities defined by

$$\beta_1=\frac{\alpha_1u_w}{2l}, \beta_2=\frac{\alpha_2u_w}{2l}, \beta_3=\frac{\alpha_3u_w}{2l}, Pr=\frac{\nu_f}{\alpha_f}, \alpha=\frac{V_{ref}}{U_{ref}}, M^2=\frac{2l\sigma B_0^2}{(\rho c_p)_f u_w},$$
$$Pr=\frac{\mu_f c_p}{k_f}, \delta_r=\frac{2lk_r}{u_w}, Ec=\frac{U_{ref}^2}{c_p(T_w-T_\infty)}, Q=\frac{2lQ_1}{(\rho c_p)_f u_w}, Rd=\frac{4\sigma^*T_\infty^3}{k^*k_f}, \quad (2.26)$$
$$Sc=\frac{\nu_f}{D_B}, Pe=\frac{bW_c}{D_N}, Sc_b=\frac{\nu_f}{D_N}, \delta_n=\frac{N_\infty}{N_w-N_\infty}, Nb=\frac{\tau D_B(C_w-C_\infty)}{\alpha_f},$$
$$Nb=\frac{\tau D_T(T_w-T_\infty)}{T_\infty\alpha_f}, s_1=\frac{a_1}{b_1}, s_2=\frac{a_2}{b_2}, s_3=\frac{a_3}{b_3}.$$

The Nusselt, Sherwood and Density numbers computation given below

$$Nu_x=\frac{q_h}{k_f(T_w-T_\infty)}, Sh_x=\frac{q_m}{D_B(C_w-C_\infty)}, Nn_x=\frac{q_n}{D_N(N_w-N_\infty)}, \quad (2.27)$$

where q_h, q_m, q_n are heat, mass and microorganism fluxes respectively

$$q_h=-k_f\left(1+\frac{16\sigma T_\infty^3}{3k_fk^*}\right)\frac{\partial T}{\partial z}|_{z=0}, q_m=-D_B\frac{\partial C}{\partial z}|_{z=0}, q_n=-D_N\frac{\partial N}{\partial z}|_{z=0}, \quad (2.28)$$

The dimensionless numbers final expressions are given by

$$Ra_x^{-\frac{1}{2}}Nu_x=-\left(\frac{1}{1-s_1}\right)\left(1+\frac{4}{3}Rd\right)\theta'(0), Ra_x^{-\frac{1}{2}}Sh_x=-\left(\frac{1}{1-s_2}\right)\phi'(0),$$
$$Ra_x^{-\frac{1}{2}}Nn_x=-\left(\frac{1}{1-s_3}\right)\chi'(0), \quad (2.29)$$

with Reynolds number

$$Ra_x=\frac{U_{ref}e^{\left(\frac{x+y}{l}\right)}}{\nu_f}$$

.

https://doi.org/10.58715/bangmodjmcs.2022.8.6

3. Solution Methodology

The Homotopy analysis method (HAM) was chosen to solved the system of equations 2.20 − 2.24 as it has an advantage over other techniques. Liao [38–40] proposed this techniques as a strong semi-analytical method. It is frequently applicable, even when there exist a relatively restricted parameters and / or otherwise(one of key requirement for perturbation techniques). It is capable of solving nonlinear problems (both strongly and weakly linearity). It provides variety of choices of choosing the initial functions of the solutions and flexibility in deciding the operators (linear). Moreover, itgives an easy way for making sure that, the series solutions convergence.
Choosing the initial guesses and the solutions' linear operators $f(\zeta)$,$h(\zeta)$,$\theta(\zeta)$, $\phi(\zeta)$ and $\chi(\zeta)$ as

$$f_0(\zeta) = 1 - e^{-\zeta},\ h_0(\zeta) = \alpha(1 - e^{-\zeta}),\ \ \theta_0(\zeta) = (1 - s_1)e^{-\zeta},$$
$$\phi_0(\zeta) = (1 - s_2)e^{-\zeta},\ \chi_0(\zeta) = (1 - s_3)e^{-\zeta}. \tag{3.1}$$

and

$$\bar{\mathcal{L}}_f[f] = f''' - f',\ \ \bar{\mathcal{L}}_h[h] = h''' - h',\ \ \bar{\mathcal{L}}_\theta[\theta] = \theta'' - \theta,$$
$$\bar{\mathcal{L}}_\phi[\phi] = \phi'' - \phi,\ \ \bar{\mathcal{L}}_\chi[\chi] = \chi'' - \chi, \tag{3.2}$$

fulfilling the following properties

$$\bar{\mathcal{L}}_f(B_1 + B_2e^{\zeta} + B_3e^{-\zeta}) = 0,\ \ \bar{\mathcal{L}}_f(B_4 + B_5e^{\zeta} + B_6e^{-\zeta}) = 0, \bar{\mathcal{L}}_\theta(B_7e^{\zeta} + B_8e^{-\zeta}) = 0,$$
$$\bar{\mathcal{L}}_\phi(B_9e^{\zeta} + B_{10}e^{-\zeta}) = 0,\ \ \bar{\mathcal{L}}_\chi(B_{11}e^{\zeta} + B_{12}e^{-\zeta}) = 0 \tag{3.3}$$

with $B_i(i = 1, ..., 12,)$ arbitrary constants. Problems' equivalent zeroth order form is

$$(1 - \varrho)\bar{\mathcal{L}}_f[f(\zeta;\varrho) - f_0(\zeta)] = \varrho\bar{h}_f\bar{\mathcal{N}}_f[f(\zeta,\varrho), h(\zeta,\varrho), \theta(\zeta,\varrho), \phi(\zeta,\varrho), \chi(\zeta,\varrho)], \tag{3.4}$$
$$(1 - \varrho)\bar{\mathcal{L}}_h[h(\zeta;\varrho) - h_0(\zeta)] = \varrho\bar{h}_h\bar{\mathcal{N}}_h[h(\zeta,\varrho), f(\zeta,\varrho), \theta(\zeta,\varrho), \phi(\zeta,\varrho), \chi(\zeta,\varrho)], \tag{3.5}$$
$$(1 - \varrho)\bar{\mathcal{L}}_\theta[\theta(\zeta;\varrho) - \theta_0(\zeta)] = \varrho\bar{h}_\theta\bar{\mathcal{N}}_\theta[\theta(\zeta,\varrho), f(\zeta,\varrho), h(\zeta,\varrho), \phi(\zeta,\varrho)], \tag{3.6}$$
$$(1 - \varrho)\bar{\mathcal{L}}_\phi[\phi(\zeta,\varrho) - \phi_0(\zeta)] = \varrho\bar{h}_\phi\bar{\mathcal{N}}_\phi[\phi(\zeta,\varrho), \theta(\zeta,\varrho), f(\zeta,\varrho), h(\zeta,\varrho)], \tag{3.7}$$
$$(1 - \varrho)\bar{\mathcal{L}}_\chi[\chi(\zeta,\varrho) - \chi_0(\zeta)] = \varrho h_\chi\bar{\mathcal{N}}_\chi[\chi(\zeta,\varrho), \phi(\zeta,\varrho), f(\zeta,\varrho), h(\zeta,\varrho)], \tag{3.8}$$

with the embedding parameter $\varrho \in [0, 1]$, and operators (nonlinear) $\bar{\mathcal{N}}_f$, $\bar{\mathcal{N}}_h$, $\bar{\mathcal{N}}_\theta$, $\bar{\mathcal{N}}_\phi$ and $\bar{\mathcal{N}}_\chi$ obtained their expressions through equations 2.20 to 2.24.
The m order deformation expressions are given as

$$\bar{\mathcal{L}}_f[f_m(\zeta,\varrho) - \eta_m f_{m-1}(\zeta)] = \bar{h}_f\mathcal{R}_{f,m}(\zeta), \tag{3.9}$$
$$\bar{\mathcal{L}}_h[h_m(\zeta,\varrho) - \eta_m h_{m-1}(\zeta)] = \bar{h}_h\mathcal{R}_{h,m}(\zeta), \tag{3.10}$$
$$\bar{\mathcal{L}}_\theta[\theta_m(\zeta,\varrho) - \eta_m \theta_{m-1}(\zeta)] = \bar{h}_\theta\mathcal{R}_{\theta,m}(\zeta), \tag{3.11}$$
$$\bar{\mathcal{L}}_\phi[\phi_m(\zeta,\varrho) - \eta_m \phi_{m-1}(\zeta)] = \bar{h}_\phi\mathcal{R}_{\phi,m}(\zeta), \tag{3.12}$$
$$\bar{\mathcal{L}}_\chi[\chi_m(\zeta,\varrho) - \eta_m \chi_{m-1}(\zeta)] = \bar{h}_\chi\mathcal{R}_{\chi,m}(\zeta), \tag{3.13}$$

$$\eta_m = \begin{cases} 1, & \text{if } m > 1 \\ 0, & \text{if } m \leq 1, \end{cases} \tag{3.14}$$

https://doi.org/10.58715/bangmodjmcs.2022.8.6

Table 1. Convergent solutions for some order approximations.

order of approximations	$-f''(0)$	$-h''(0)$	$-\theta'(0)$	$-\phi'(0)$	$-\chi'(0)$
1	0.92593	0.15545	0.67333	0.44933	0.59596
5	0.93095	0.16071	0.62041	0.35816	0.59583
10	0.93106	0.16088	0.61353	0.35541	0.59575
15	0.93103	0.16089	0.61214	0.35486	0.59575
25	0.93103	0.16089	0.61177	0.35471	0.59575
30	0.93103	0.16089	0.61163	0.35465	0.59575
35	0.93103	0.16089	0.61163	0.35465	0.59575

the expressions of $\mathcal{R}_f^m$, $\mathcal{R}_h^m$, $\mathcal{R}_\theta^m$, $\mathcal{R}_\phi^m$, $\mathcal{R}_\chi^m$ is computed through equations 2.20 to 2.24. The general solutions are

$$f_m(\zeta) = f_m^*(\zeta) + B_1 + B_2 e^{\zeta} + B_3 e^{-\zeta}, \tag{3.15}$$

$$h_m(\zeta) = h_m^*(\zeta) + B_4 + B_5 e^{\zeta} + B_6 e^{-\zeta}, \tag{3.16}$$

$$\theta_m(\zeta) = \theta_m^*(\zeta) + B_7 e^{\zeta} + B_8 e^{-\zeta}, \tag{3.17}$$

$$\phi_m(\zeta) = \phi_m^*(\zeta) + B_9 e^{\zeta} + B_{10} e^{-\zeta}, \tag{3.18}$$

$$\chi_m(\zeta) = \chi_m^*(\zeta) + B_{11} e^{\zeta} + B_{12} e^{-\zeta}, \tag{3.19}$$

with the special solutions $f_m^*, h_m^*, \theta_m^*, \phi_m^*, \chi_m^*$.

3.1. Analysis of Convergence of the solutions

Clearly, the convergence control parameter $\bar{h}$ is appeared in the series solutions obtained by the homotopy analysis method. This parameter governs the HAM solution's convergence rate of approximation as Liao pointed out. Convergent solutions with the values of the following parameters $s_1 = s_2 = s_3 = \delta_r = \delta_n = 0.1; \beta_1 = \beta_2 = Q = 0.2; \beta_3 = M = Sc_b = \alpha = Rd = 0.3; Ec = 0.6; Nb = \tau = 0.5; Nt = 0.4; Pr = Pe = 0.7$ for some order approximations given in Table 1. Figures 2 and 3 displayed the $\bar{h}$-curves plots with convergence regions obtained as $-1.0 \leqslant \bar{h}_f \leqslant 0$, $-1.2 \leqslant \bar{h}_h \leqslant 0.8$, $-1.1 \leqslant \bar{h}_\theta \leqslant 0.1$, $-1.25 \leqslant \bar{h}_\phi \leqslant 0.26$, and $-1.2 \leqslant \bar{h}_\chi \leqslant 0.8$.

4. Results and Discussion

Through Figures 434, this segment discusses important characteristics of non-dimensional parameters on velocities, temperature, concentration and microorganisms profiles, and heat-mass and density transport rates. Figure 4 depicted the effect of Deborah number with respect to relaxation time β_1 on velocity profile along the x direction. Deborah number and relaxation time are inextricably linked. As an outcome, a longer relaxation time results in a higher Deborah number, which is induced by fluid flow resistance with velocity decrease. In contrast, both β_1 and Deborah number with respect to retardation time β_2 have opposite effect on the x directions velocity. According to the meaning of β_2, it is related directly to the retardation time and identified as delay response on the applied force or elasticity delay. Figure 5 depicts that the velocity increases as the parameter β_2 increases. The effect of β_1 on the y direction's velocity profile is demonstrated in Figure 6. As β_1 increases, the velocity and boundary layer thins along this direction. It is seen as important as a result of a slower process of recovery being observed towards greater time

https://doi.org/10.58715/bangmodjmcs.2022.8.6

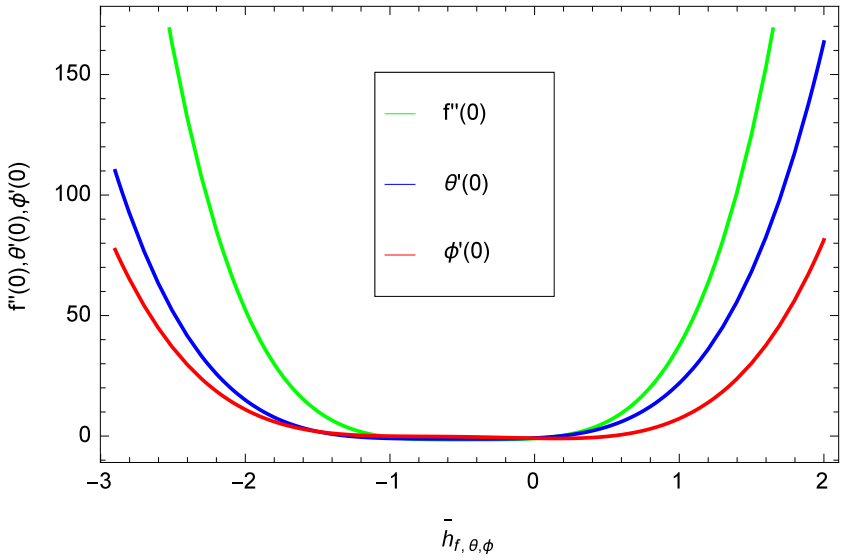

FIGURE 2. $\bar{h}$-curve of $f(\zeta), \theta(\zeta)$ and $\phi(\zeta)$.

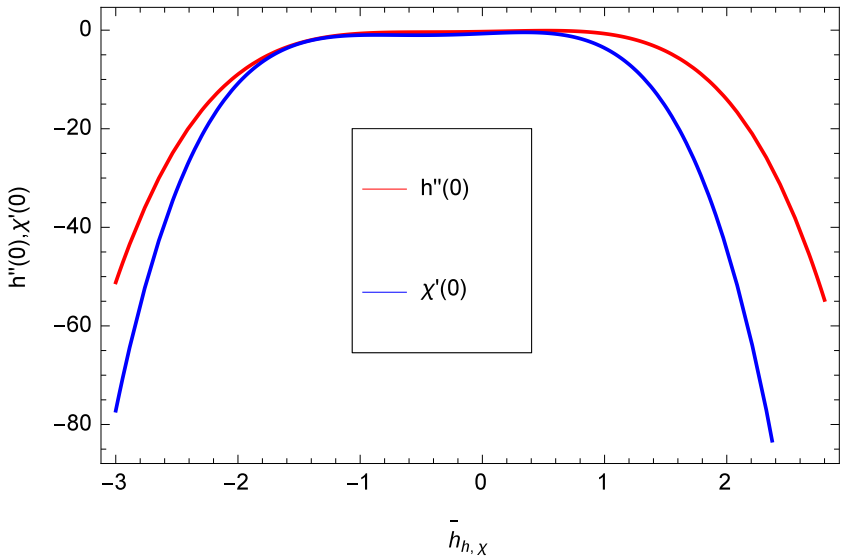

FIGURE 3. $\bar{h}$-curve of $h(\zeta)$ and $\chi(\zeta)$.

https://doi.org/10.58715/bangmodjmcs.2022.8.6

of relaxation, which results in a slower thickening of the boundary layers. The influences of β_2 on y direction's velocity profile shown in Figure 7. When β_2 is increased in this case, the y direction's velocity and boundary layer thickness improved. Figure 8 depicts that, x direction's velocity as decreasing velocity function for magnetic field parameter M. A Lorentz force produced via induced circumferential magnetic field opposes the flow rate along this direction, as a result of this the velocity is decreases. Figure 9 and 10 depicts the role of velocity ratio parameter α on the velocity along x and y directions respectively. It demonstrates that for larger α, the boundary layer thickens in the $x-$direction$x$ direction's velocity, whereas for smaller α, the boundary layer thins in the $y-$ direction's velocity.

Figure 11 shows the role of β_1 on temperature profile. Because the fluid temperature is proportional to relaxation time, the greater β_1 causes in the temperature increasing and, thus, the boundary layer (thermal) thickening. Role of β_2 on temperature profile is shown in Figure 12. This has been discovered that as β_2 increases, the temperature decreases. Figure 13 depicts the temperature variation as a function of M, demonstrating how an electric current in the applied magnetic field creates a Lorentz forces. This forces withstands the fluid's motion, resulting in the production of extra heat, which raises temperature and boundary layer thickens. Figure 14 depicts the behavior of thermophoretic parameter Nt on the temperature profile. When Nt is increased, temperature enhanced and the boundary layer (thermal) thickens. Figure 15 depicts the effect of Brownian motion parameter Nb on θ. When the value of Nb increases, both temperature and the boundary layer (thermal) thickens. Physically, Under thermophoretic force participation, nanoparticles adjacent to the heated boundary are driven toward the colder material at ambient temperature. As a result, the thermal-layer is expected to thicken as the thermophoretic element occurs. Furthermore, as Nb increases, the irregular motion of material elements improves. The role of thermal radiation parameter Rd on temperature profile is shown in Figure 16. The upsurge in temperature is observed as the values of Rd increment. Because when the values Rd are high, further heat is transported to the nanofluid. Figure 17 depicts the influence of the Pr on temperature profile. As Pr increases, the temperature decreases. Normally, greater Pr have lower diffusivity (thermal), while smaller Pr have greater diffusivity (thermal). This decrease in thermal diffusivity results in temperature decrease and the boundary layer (thermal) thickens. Figure 18 depicts the variation of temperature profile for various values of Eckert number Ec. The Ec define the connection between flow kinetic energy and the heat enthalpy difference. As a result, increasing the Ec causes an increase in kinetic energy. Furthermore, it is well understood that temperature refers to kinetic energy average. Because of this, the fluid's temperature rises as Ec increases. The effect of heat generation/absorption parameter Q on temperature profile is shown in Figure 19. It demonstrates that as the value of Q increases, so does the temperature. It occurs as a result of an increase in the values of Q, which implies that more heat energy is supplied to the flow, causing the temperature to rise. Figure 20 depicts that as thermal stratification parameter s_1 increases, so does the temperature. Because of the stratification implications, the critical temperature of fluid along the sheets and away from sheets may decrease, resulting in a thinner thermal boundary layer and a weakened the flow temperature. It further shows that an increase in free-stream temperature or even a decline in nanofluid surface temperature. In actuality, stratification has an influence on nanofluid temperature because it raises ambient

https://doi.org/10.58715/bangmodjmcs.2022.8.6

temperature or causes a decrease in surface temperature. These activity is frequently observed when heat transfers out of a warmer region to a cooler region.

Figure 21 depicts the role of chemical reaction parameter δ_r on the concentration profile. It shows that the concentration decreases as the chemical reaction parameter δ_r increases, whereas the velocities, and the temperature are unaffected by δ_r. Figure 22 shows that the concentration decreases as Brownian motion parameter Nb increases. Figure 23 shows the concentration variation for different Nt. The concentration and the boundary layer thickness are both intensifying when the values of Nt increases. Figure 24 shows that as the Schmidt number Sc increases, concentration decrease rapidly, inferring that less diffusion happens through use of mass transfer. This is because, the higher values of Sc correlated with a decline in chemical molecular diffusing, while smaller values of Sc produce a much concentration drop from the surface. Sc has a physical relationship that is inversely proportional to mass diffusivity. Lower mass diffusivity results from higher Sc. larger value of Sc indicates a lower mass diffusivity. The concentration of the nanoparticle decreases due to the lower mass diffusivity. Figure 25 depicts the variation in concentration by increasing the values of mass stratification parameter s_2. The figure shows that as s_2 values increase, the concentration decreases. Because the fluid closer to the sheet's boundary, its concentration may be lower than that of the surrounding medium. Figure 26 depicts the effect of Peclet number Pe on the motile density profile. It has been observed that as the values of Pe increase, than the motile density decreases. As a result, the density of motile microorganisms decrease the speed and/or diffusivity of microorganisms does. However,lower microorganism concentrations in the boundary layer, as well as an increase in the motile microorganism mass transfer rate, will result as an outcome. As shown in Figure 27, increased the Schmidt number of bioconvection Sc_b affect the motile density to decrease. As shown in Figure 28, the motile density decreases as the values bioconvection constant δ_n increase. Figure 29 indicates that greater s_3 values decrease the motile density. However, gyrotaxis to the current analysis of bioconvection in a stratified system, could provide additional insight into this interesting trend phenomenon. The method's consistency has been confirmed by comparing it to the results reported in Khan et al. [17], Table 2 displayed the result. The numerical results for Nusselt number Nu and Sherwood number Sh forvariousphysical parametersare shown in Table 3. Nu rise when β_2, Rd, s_1, and Pr increase, while it falls down when β_1, Q, M, and Ec increase. However, the table shows that as the parameters Rd, Sc, Q, and β_2 increase, Sh is also increases, and as β_1, s_2, and δ_r increase, Sh decreases. The microorganism transfer rate increases for some values of some parameters, as shown in Table 4. Figure 31 gives influence of β_1 and α on Nu. Observations shows that Nu rises with the escalating values of α. Increasing β_1, on the other hand, exhibit opposite trend. Figure 32 show the role of Pr and β_3 on the Nu. Observations shows that Nu rises with escalating values of Pr. Increasing the values of β_3 on the other hand exhibit the opposite trend, this shows similar outcomes with the result obtained in figure 16 of [8]. Figure 33 depicts the influence of Nb and Sc on Sh. According to this graph, Sh increase for Nb and Sc which shows similar result with figure 13 of [11]. Nn varied in relation for different values of s_3 and δ_n. Figure 34 shows that Nn increases by increasing δ_n while by increasing s_3 shows the opposite pattern.

https://doi.org/10.58715/bangmodjmcs.2022.8.6
TaCS Publications
Bangmod J-MCS 2022

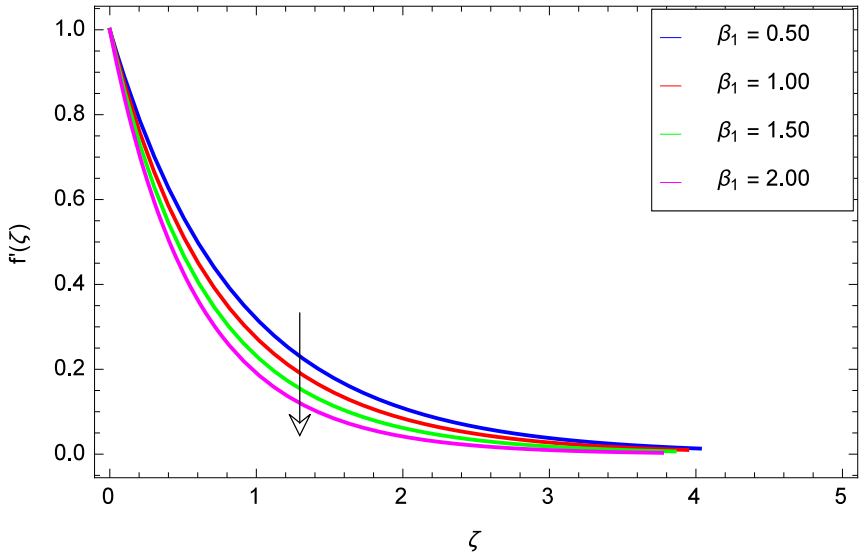

FIGURE 4. Influence of β_1 on $f'(\zeta)$.

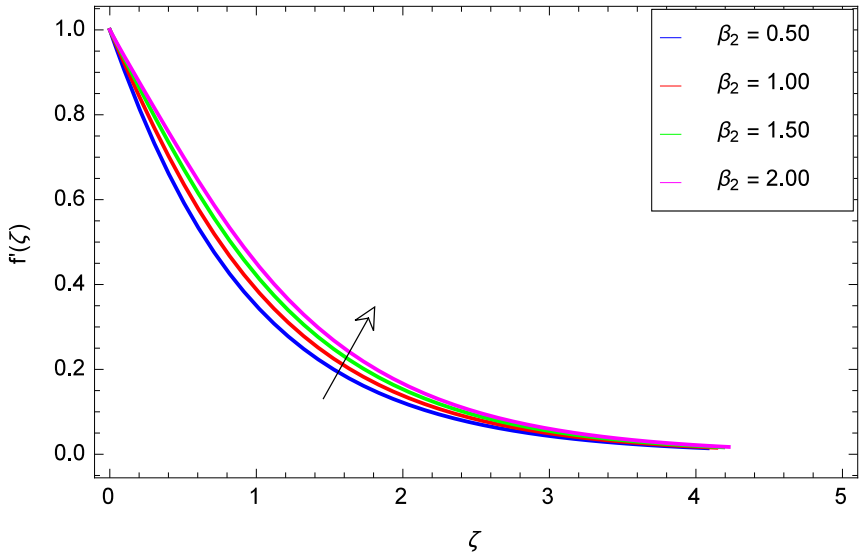

FIGURE 5. Influence of β_2 on $f'(\zeta)$.

https://doi.org/10.58715/bangmodjmcs.2022.8.6
Bangmod J-MCS 2022

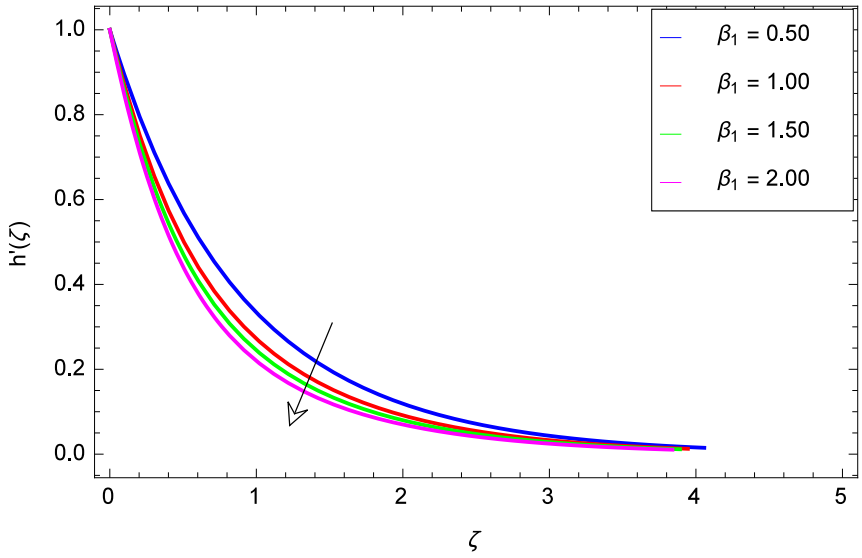

FIGURE 6. Influence of β_1 on $h'(\zeta)$.

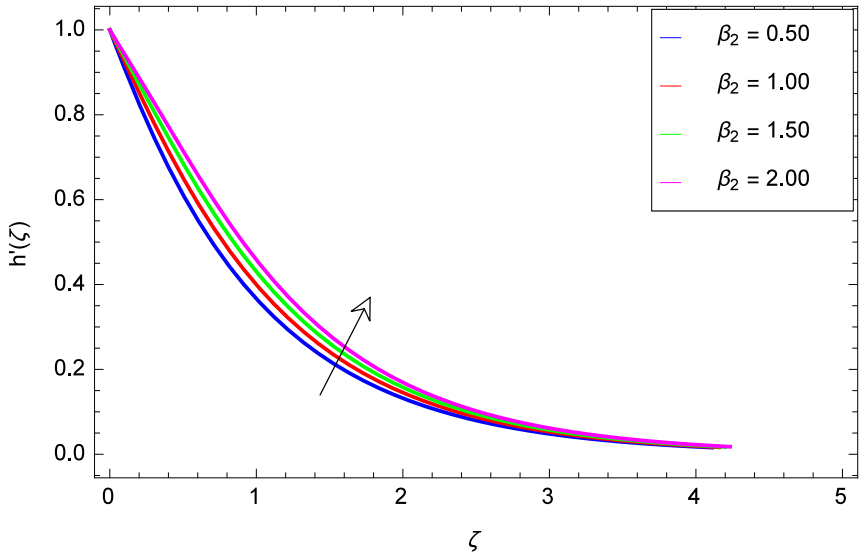

FIGURE 7. Influence of β_2 on $h'(\zeta)$.

https://doi.org/10.58715/bangmodjmcs.2022.8.6
Bangmod J-MCS 2022

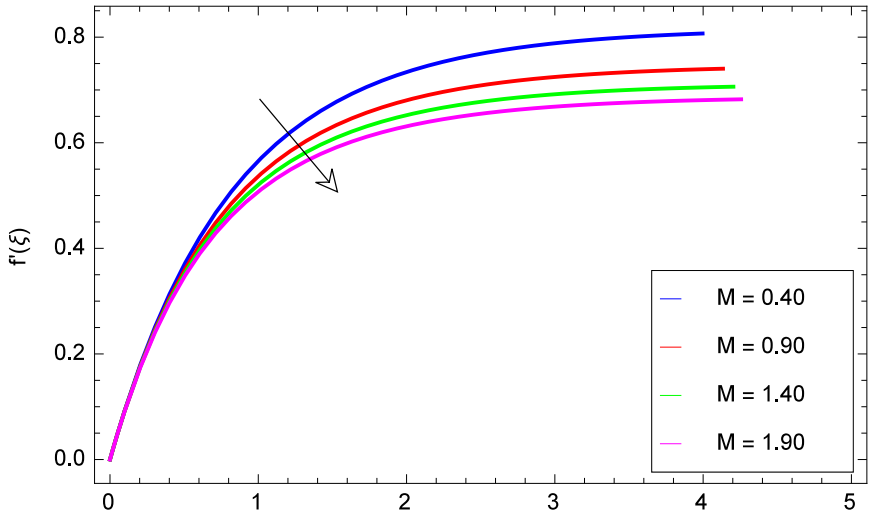

FIGURE 8. Influence of M on $f'(\zeta)$.

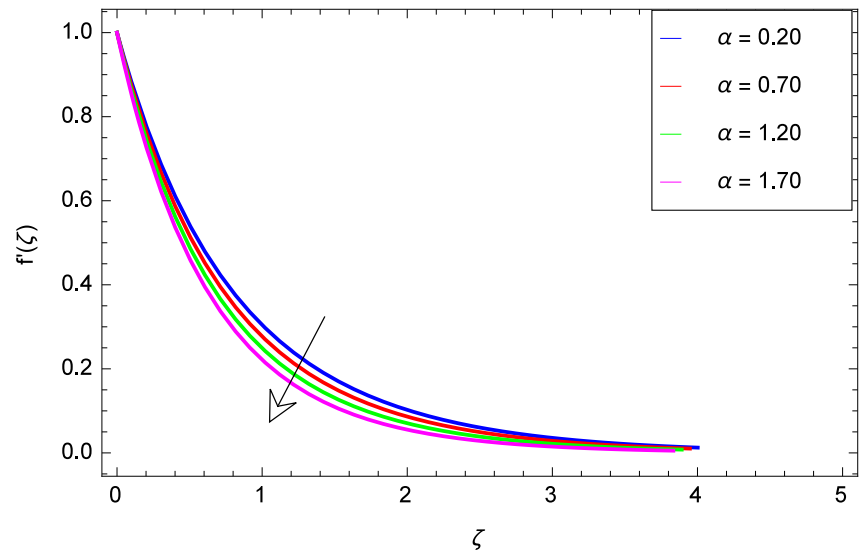

FIGURE 9. Influence of α on $f'(\zeta)$.

https://doi.org/10.58715/bangmodjmcs.2022.8.6

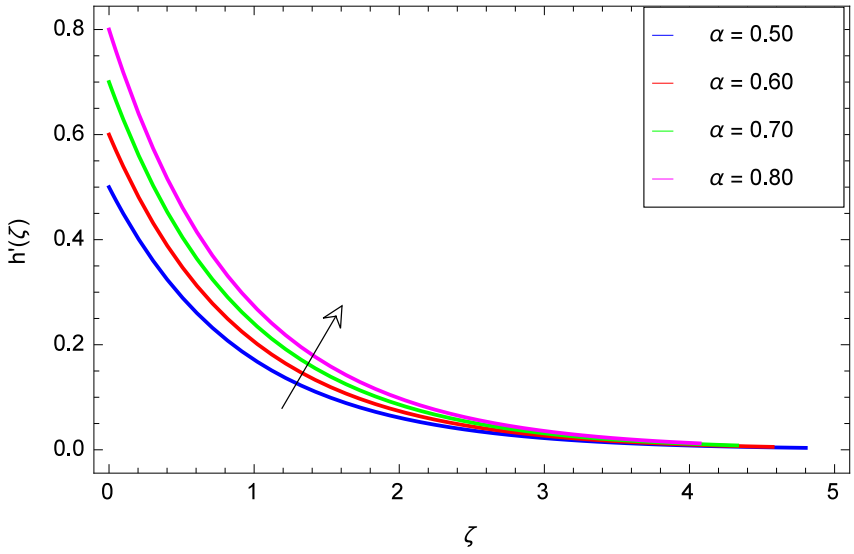

FIGURE 10. Influence of α on $h'(\zeta)$.

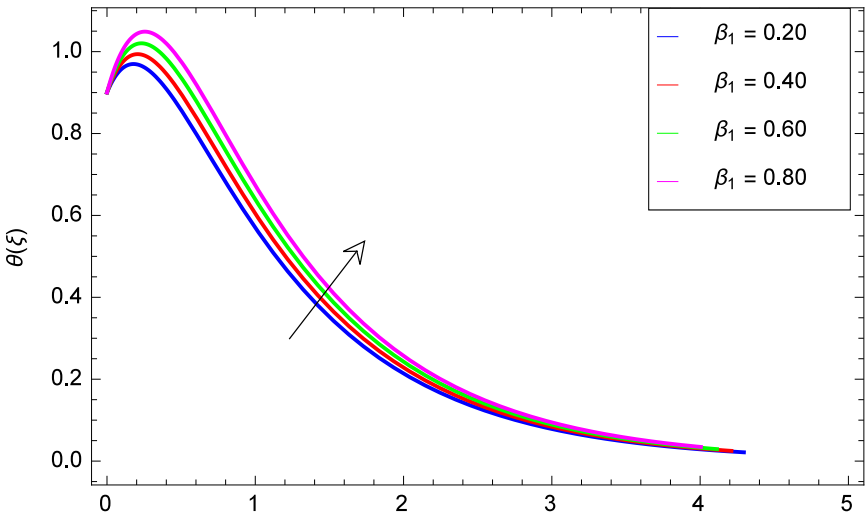

FIGURE 11. Influence of β_1 on $\theta(\zeta)$.

https://doi.org/10.58715/bangmodjmcs.2022.8.6

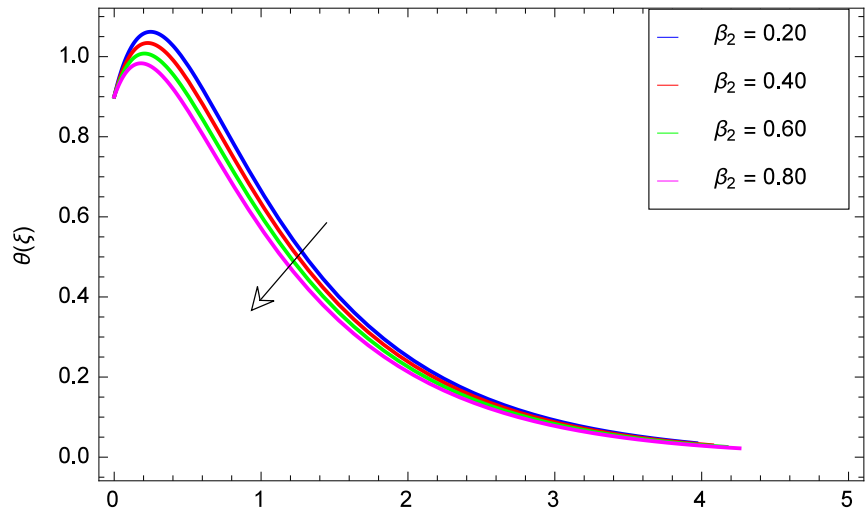

FIGURE 12. Influence of β_2 on $\theta(\zeta)$.

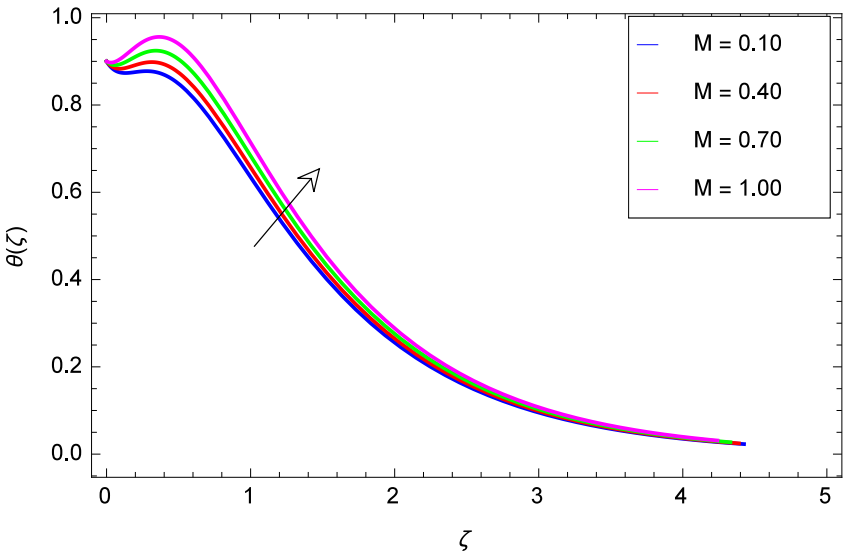

FIGURE 13. Influence of M on $\theta(\zeta)$.

https://doi.org/10.58715/bangmodjmcs.2022.8.6
Bangmod J-MCS 2022

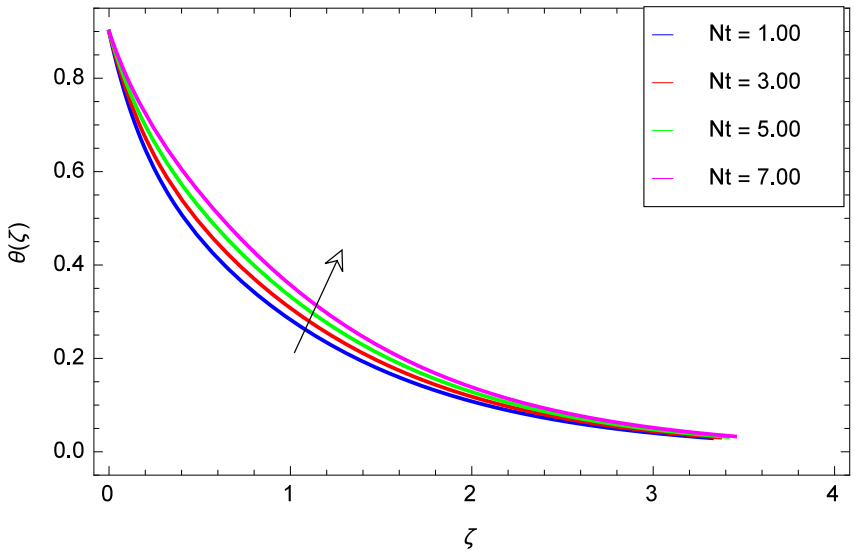

FIGURE 14. Influence of Nt on $\theta(\zeta)$.

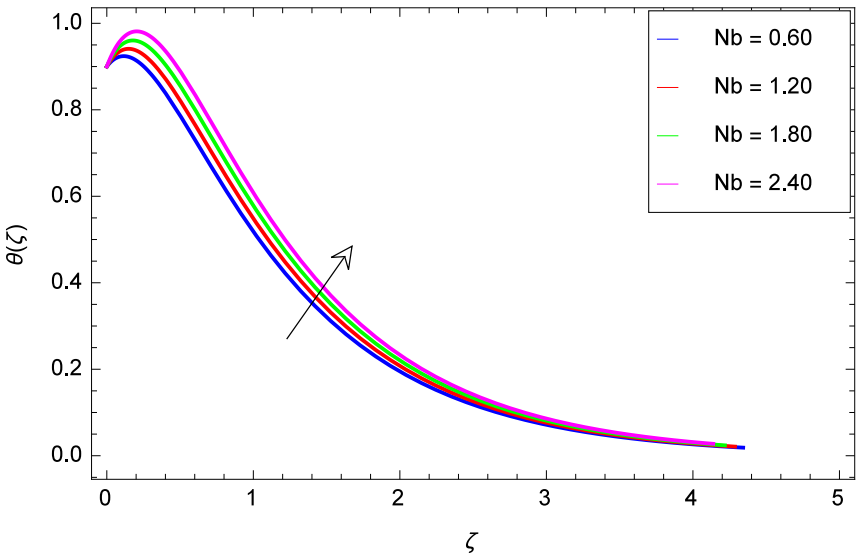

FIGURE 15. Influence of Nb on $\theta(\zeta)$.

https://doi.org/10.58715/bangmodjmcs.2022.8.6

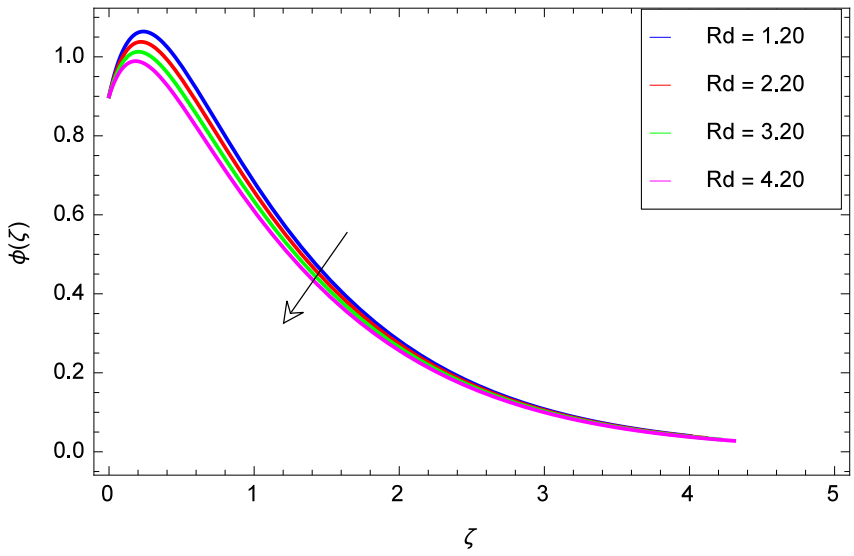

FIGURE 16. Influence of Rd on $\theta(\zeta)$.

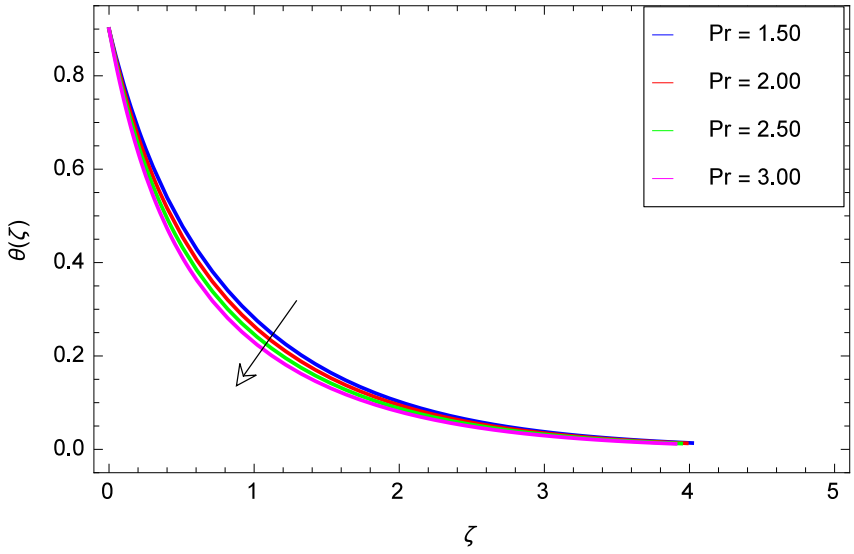

FIGURE 17. Influence of Pr on $\theta(\zeta)$.

https://doi.org/10.58715/bangmodjmcs.2022.8.6
Bangmod J-MCS 2022

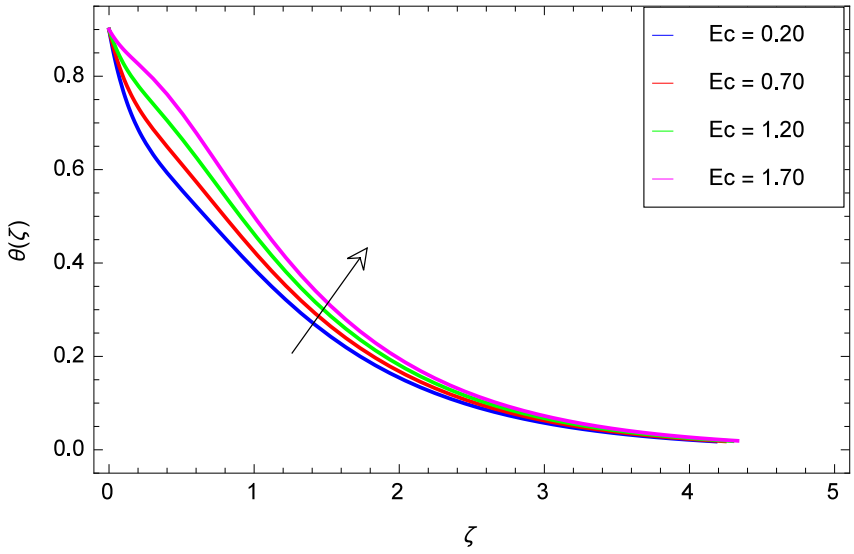

FIGURE 18. Influence of Ec on $\theta(\zeta)$.

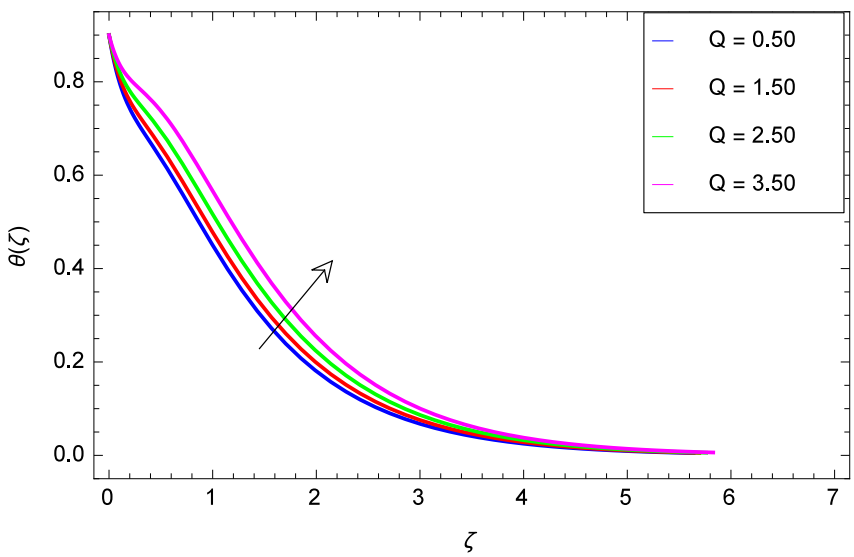

FIGURE 19. Influence of Q on $\theta(\zeta)$.

https://doi.org/10.58715/bangmodjmcs.2022.8.6
Bangmod J-MCS 2022

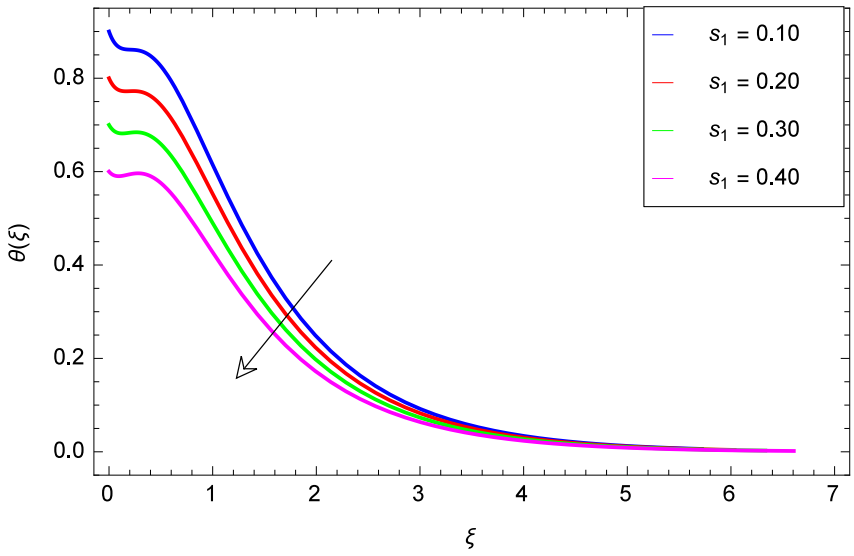

FIGURE 20. Influence of s_1 on $\theta(\zeta)$.

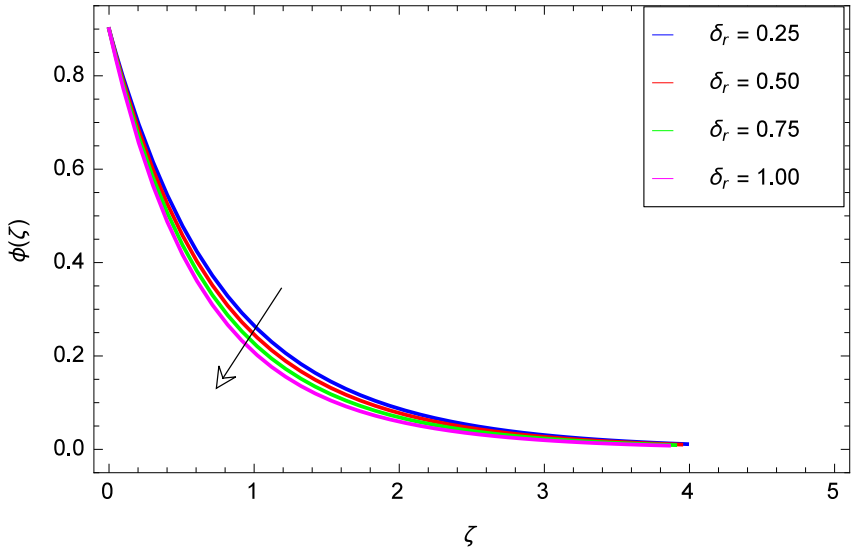

FIGURE 21. Influence of δ_r on $\phi(\zeta)$.

https://doi.org/10.58715/bangmodjmcs.2022.8.6

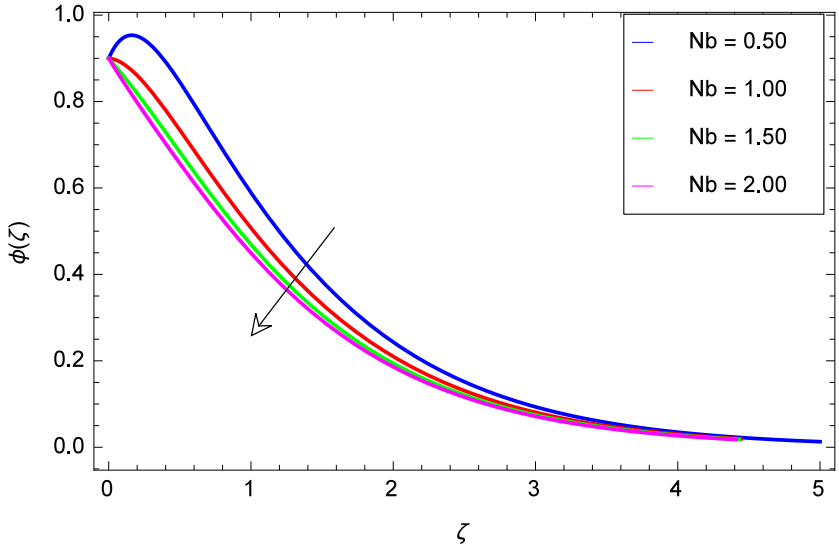

FIGURE 22. Influence of Nb on $\phi(\zeta)$.

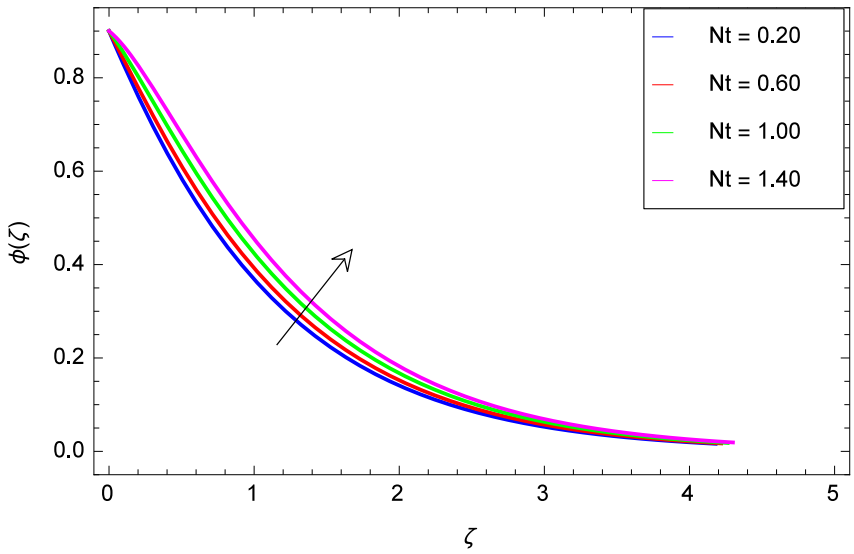

FIGURE 23. Influence of Nt on $\phi(\zeta)$.

https://doi.org/10.58715/bangmodjmcs.2022.8.6
Bangmod J-MCS 2022

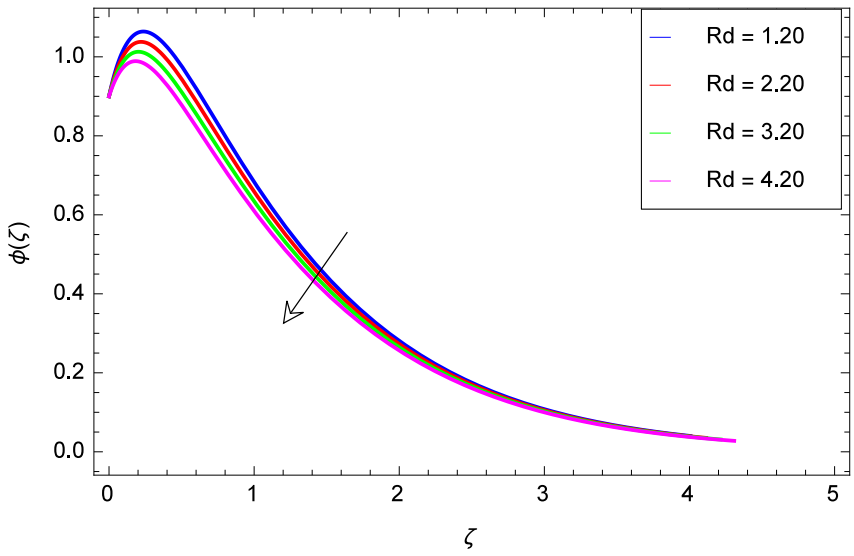

FIGURE 24. Influence of Rd on $\phi(\zeta)$.

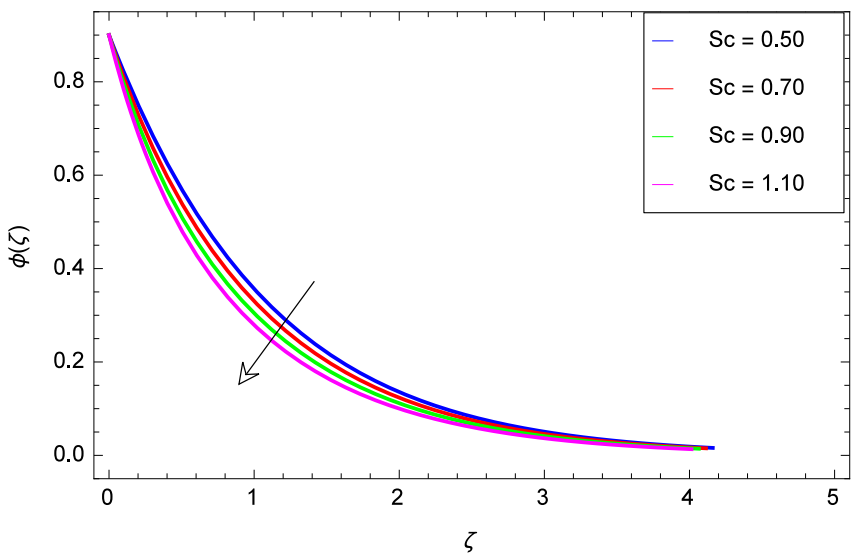

FIGURE 25. Influence of Sc on $\phi(\zeta)$.

https://doi.org/10.58715/bangmodjmcs.2022.8.6
Bangmod J-MCS 2022

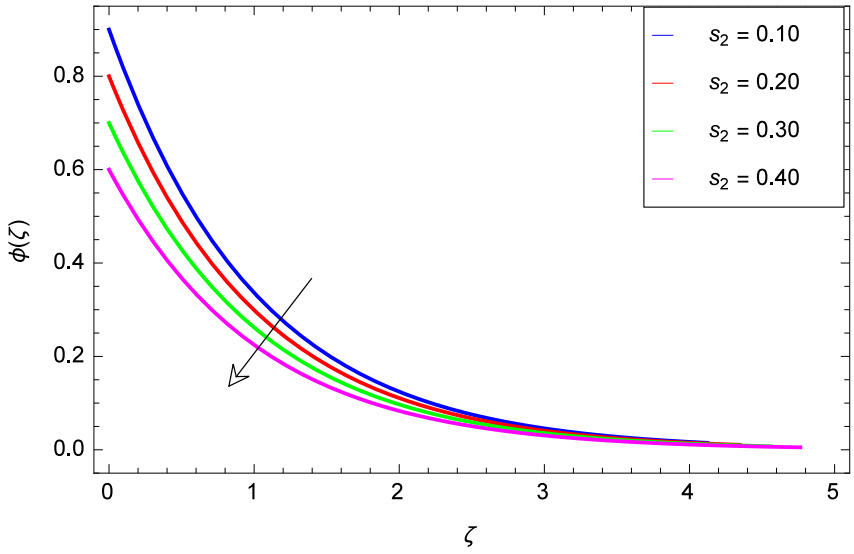

FIGURE 26. Influence of s_2 on $\phi(\zeta)$.

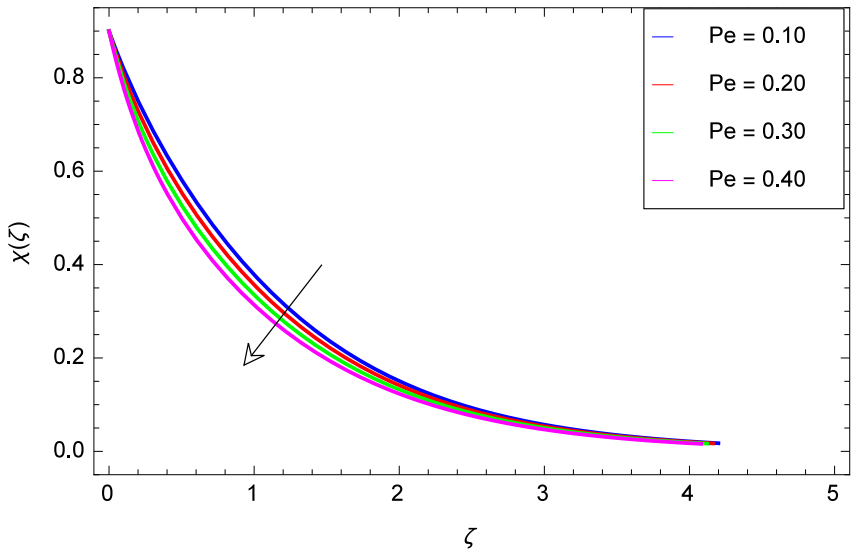

FIGURE 27. Influence of Pe on $\chi(\zeta)$.

https://doi.org/10.58715/bangmodjmcs.2022.8.6
Bangmod J-MCS 2022

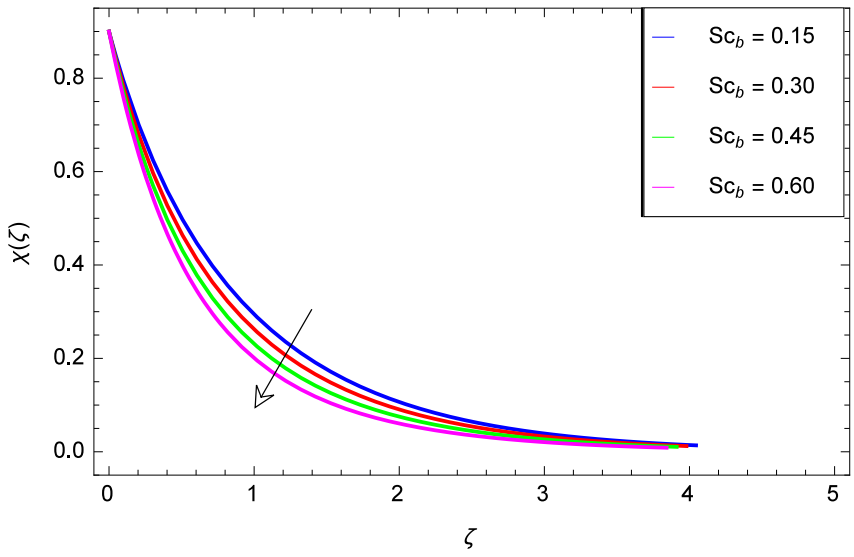

FIGURE 28. Influence of Sc_b on $\chi(\zeta)$.

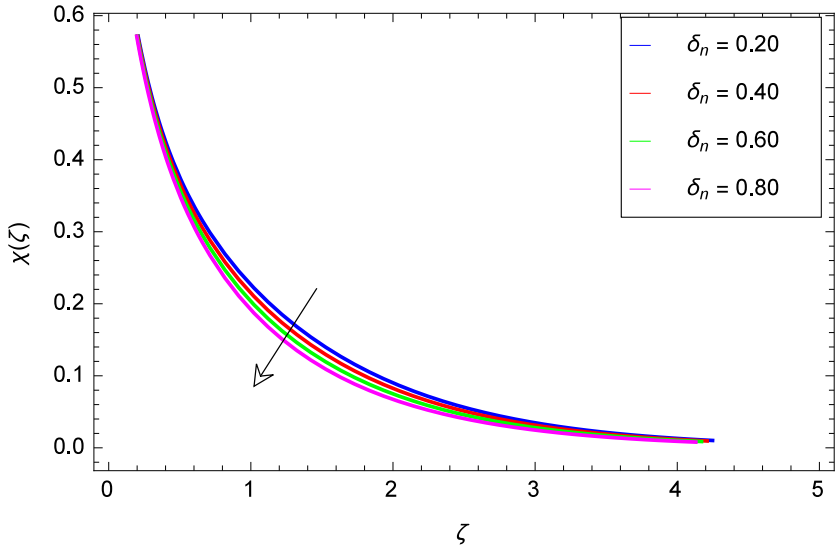

FIGURE 29. Influence of δ_n on $\chi(\zeta)$.

https://doi.org/10.58715/bangmodjmcs.2022.8.6

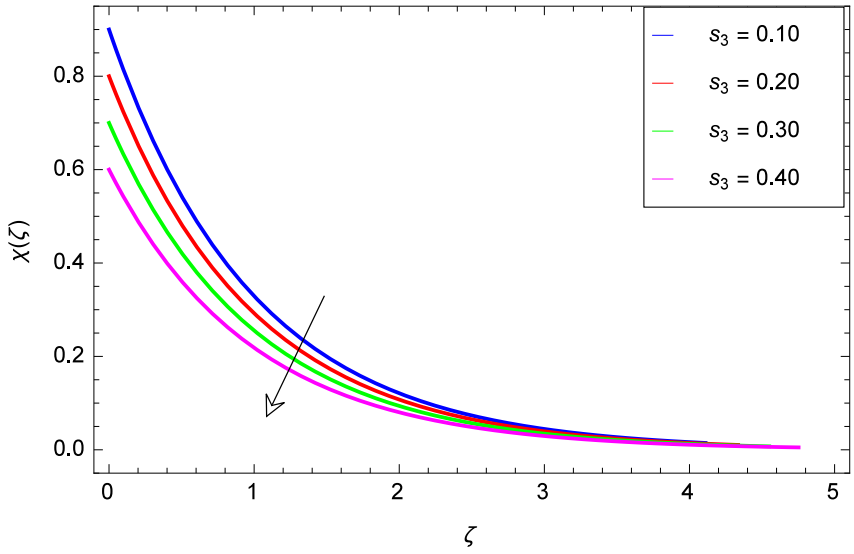

FIGURE 30. Influence of s_3 on $\chi(\zeta)$.

TABLE 2. Agreement of $-\theta'(0)$ and $-\phi'(0)$ for some values of Nb and Nt with published work.

Parameters		**Khan et al. [17]**	**present**	**Khan et al. [17]**	**present**
Nb	Nt	$-\theta'(0)$	$-\theta'(0)$	$-\phi'(0)$	$-\phi'(0)$
0.5	0.3	0.701844	0.701844	0.570216	0.570301
0.6	0.3	0.682779	0.681999	0.647005	0.647012
1.0	0.3	0.664968	0.665001	0.707544	0.707541
0.3	0.0	0.702259	0.702258	0.570572	0.570576
0.3	0.5	0.701844	0.701901	0.570216	0.570209
0.3	1.0	0.701326	0.701330	0.569771	0.569698

5. CONCLUSION

The focused of this research was the study of an Oldroyd-B nanofluid flow through an exponentially stretching sheet with thermal, mass, and microorganism stratifications conditions. The effect of thermal radiation, chemical reactions and viscousdissipation among others are taken into account. The problem was solved by HAM and the results are visualized graphically and numerically. The influence of the input parameters on heat and mass transfer was investigated. The following findings have been made:

- The impacts of β_2 are quite opposite to the impact of β_1 on both the velocities along x and y directions.
- Thermal boundary layer thickens and the temperature decreases as Pr, β_2 and s_1 increases and enhances for Q, Rd and Ec. In industrial processes, the Prandtl

https://doi.org/10.58715/bangmodjmcs.2022.8.6

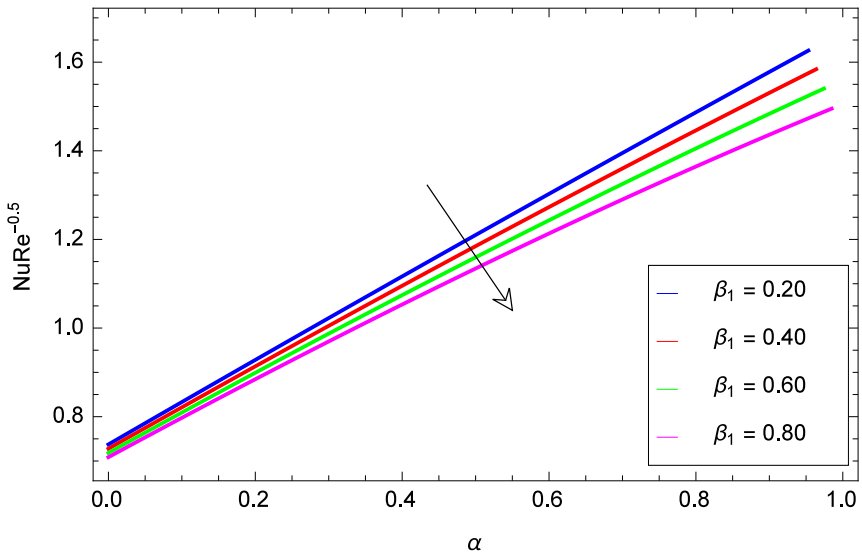

FIGURE 31. Plot of β_1 and α versus Nu.

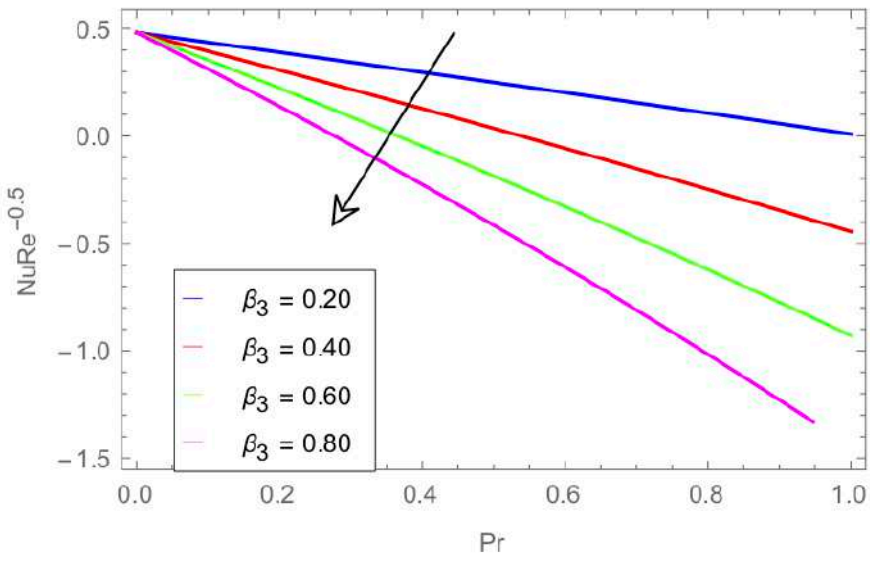

FIGURE 32. Plot of β_3 and Pr versus Nu.

https://doi.org/10.58715/bangmodjmcs.2022.8.6
Bangmod J-MCS 2022

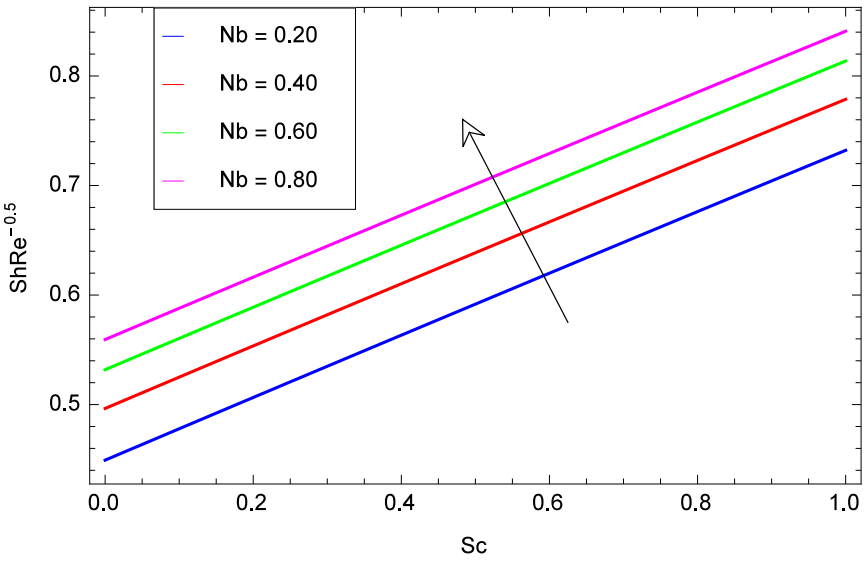

FIGURE 33. Plot of Nb and Sc versus Sh.

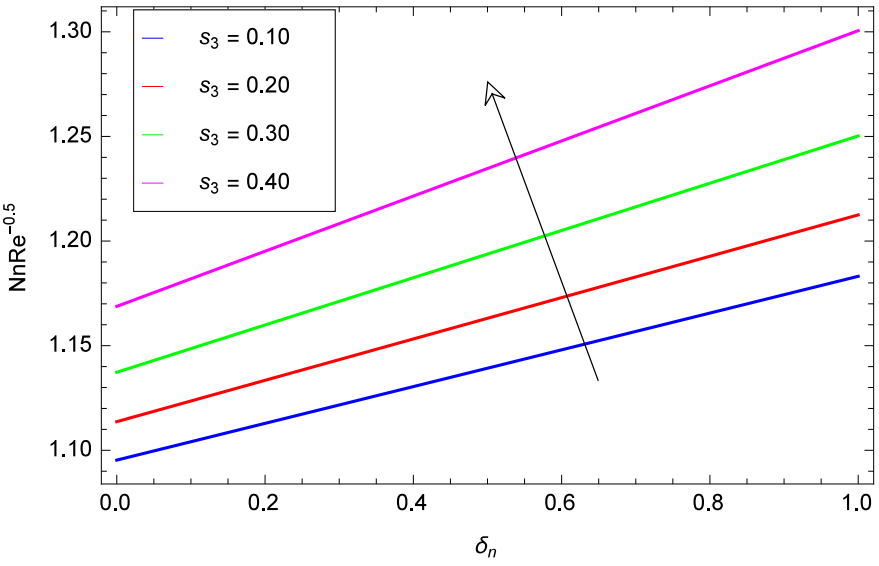

FIGURE 34. Plot of s_1 and δ_n versus Nn.

https://doi.org/10.58715/bangmodjmcs.2022.8.6

TABLE 3. Values are computed of $-\theta'(0)$ and $-\phi'(0)$ for various values of β_1, β_2, Pr, Ec, M, Rd, s_1, s_2 δ_r, Sc, Q.

β_1	β_2	Pr	Ec	M	Rd	s_1	s_2	δ_r	Sc	Q	$-\theta'(0)$	$-\phi'(0)$
0.2	0.2	0.7	0.3	0.4	0.3	0.1	0.1	0.2	0.7	0.2	0.684548	0.390173
0.3											0.680576	0.389555
0.4											0.676604	0.388937
	0.4										0.686748	0.390507
	0.6										0.688948	0.390840
	0.8										0.691148	0.391174
		2.7									1.138070	0.365571
		4.7									1.567560	0.340969
		6.7									1.973020	0.316367
			0.4								0.679220	0.390416
			0.5								0.673891	0.390658
			0.6								0.668563	0.390900
				0.5							0.684243	0.390126
				0.6							0.683921	0.390077
				0.7							0.683583	0.390026
					0.5						0.789676	0.391093
					0.7						0.887814	0.392013
					0.9						0.979412	0.392933
						0.2					0.778430	0.389825
						0.3					0.799898	0.394955
						0.4					0.828521	0.400084
							0.2				0.684548	0.333981
							0.3				0.684548	0.325225
							0.4				0.684548	0.535773
								0.4			0.684548	0.382572
								0.6			0.684548	0.375009
								0.8			0.684548	0.367485
									0.9		0.684548	0.406819
									1.1		0.684548	0.423423
									1.3		0.684548	0.439986
										0.5	0.668840	0.390898
										0.8	0.653070	0.391622
										1.1	0.637238	0.392346

number is often used to regulate the heat transfer rate [47]. The appropriate Prandtl number value is critical for controlling the rate of heat transfer in engineering and industrial processes.

- The concentration decreases as s_2, δ_r and Sc increases and the related boundary layers.
- The heat transfer rate increases for larger β_2, s_1 and Pr while it reduces by increasing β_1 and Q.
- The mass transfer rate displays a decreasing behavior for higher values of s_2 and δ_r

https://doi.org/10.58715/bangmodjmcs.2022.8.6

TABLE 4. Values are computed of $-\chi'(0)$ for various values of Pe, Sc_b, s_3, δ_n.

Pe	Sc_b	s_3	δ_n	$-\chi'(0)$
0.6	0.6	0.3	0.1	0.542835
0.8				0.573228
1				0.603722
	0.9			0.573111
	1.2			0.603300
	1.5			0.633403
		0.5		0.776957
		0.7		1.005330
		0.9		2.147210
			0.5	0.546859
			0.9	0.562954
			1.4	0.575025

- The microorganism transfer rate decreases as the values of s_3 and Pe increases.

https://doi.org/10.58715/bangmodjmcs.2022.8.6

Acknowledgments

This research project was supported by the Thailand Science Research and Innovation (TSRI) Basic Research Fund: Fiscal year 2022 under the project number FRB650048/0164. The first author is supported by the Petchra Pra Jom Klao Doctoral Scholarship Academic for Ph.D. program of King Mongkuts University of Technology Thonburi (KMUTT) [Grant No. 13/2562].

Authors contribution

A.H.U., Z.S. and W.K. formulated, solved the problem, wrote the draft. Z.S. and U.W.H. performed the investigations. A.H.U. and W.K. sketched the graphs. U.W.H. performed the supervision and provide the funding.

Statement about data

Availability exists for whole of the data.

Conflict of Interests

The authors have no conflict of interests.

References

[1] F. Irgens, Rheology and non-Newtonian fluids, New York, USA: Springer International Publishing, 2014.

[2] R.P. Chhabra, Non-Newtonian fluids: An introduction In Rheology of complex fluids, Springer, New York, (2010), 3–34.

[3] T. Hayat, A. Aziz, T. Muhammad, A. Alsaedi, Numerical treatment for DarcyForchheimer flow of nanofluid due to a rotating disk with convective heat and mass conditions, International Journal of Numerical Methods for Heat & Fluid Flow (2018).

[4] T. Hayat, A. Aziz, T. Muhammad, A. Alsaedi, Significance of homogeneoushetero-geneous reactions in Darcy-Forchheimer three-dimensional rotating flow of carbon nanotubes, Journal of Thermal Analysis and Calorimetry 139(2020) 183–195

[5] T. Hayat, A. Aziz, A. Alsaedi, Analysis of entropy production and activation energy in hydromagnetic rotating flow of nanoliquid with velocity slip and convective conditions, Journal of Thermal Analysis and Calorimetry 146(6)(2021) 2561–2576

[6] I. Ullah, T. Hayat, A. Aziz, A. Alsaedi, Significance of Entropy Generation and the Coriolis Force on the Three-Dimensional Non-Darcy Flow of Ethylene-Glycol Conveying Carbon Nanotubes (SWCNTs and MWCNTs), Journal of Non-Equilibrium Thermodynamics 47(1)(2022) 61–75.

[7] J.G. Oldroyd, On the formulation of rheological equations of state. Proceedings of the Royal Society of London. Series A. Mathematical and Physical Sciences 200(1063)(1950) 523–41.

[8] D. Lu, M. Ramzan, M. Bilal, J.D. Chung, U. Farooq, S. Tahir, On three-dimensional MHD Oldroyd-B fluid flow with nonlinear thermal radiation and homogeneoushetero-geneous reaction, Journal of the Brazilian Society of Mechanical Sciences and Engineering, 40(8)(2018) 1–11.

[9] Y. Zhang, B. Yuan, Y. Bai, Y. Cao, Y. Shen, Unsteady Cattaneo-Christov double diffusion of Oldroyd-B fluid thin film with relaxation-retardation viscous dissipation and relaxation chemical reaction, Powder Technology 338(2018) 975–82.

https://doi.org/10.58715/bangmodjmcs.2022.8.6

[10] I. Tlili, H. Waqas, A. Almaneea, S.U. Khan, M. Imran, Activation energy and second order slip in bioconvection of Oldroyd-B nanofluid over a stretching cylinder: a proposed mathematical model, Processes 7(12)(2019) 914.
[11] M. Waqas, T. Hayat, A. Alsaedi, W.A. Khan, Analytical evaluation of Oldroyd-B nanoliquid under thermo-solutal Robin conditions and stratifications, Computer Methods and Programs in Biomedicine 196(2020) 105474.
[12] A.H. Usman, N.S. Khan, U.W. Humphries, Z. Ullah, Q. Shah, P. Kumam, P. Thounthong, W. Khan, A. Kaewkhao, A. Bhaumik, Computational optimization for the deposition of bioconvection thin Oldroyd-B nanofluid with entropy generation, Scientific reports 11(1)(2021) 1–23.
[13] S.U. Choi, J.A. Eastman, Enhancing thermal conductivity of fluids with nanoparticles, Argonne National Lab., IL (United States), 1995.
[14] J. Buongiorno, Convective transport in nanofluids, ASME J. Heat Trans. 128(2006) 240–250.
[15] K.G. Kumar, G.K. Ramesh, B.J. Gireesha, R.S. Gorla, Characteristics of Joule heating and viscous dissipation on three-dimensional flow of Oldroyd-B nanofluid with thermal radiation, Alexandria Engineering Journal 57(3)(2018) 2139–49.
[16] M. Irfan, M. Khan, W.A. Khan, M. Sajid, Thermal and solutal stratifications in flow of Oldroyd-B nanofluid with variable conductivity, Applied Physics A 124(10)(2018) 1–11.
[17] S.U. Khan, A. Rauf, S.A. Shehzad, Z. Abbas, T. Javed, Study of bioconvection flow in Oldroyd-B nanofluid with motile organisms and effective Prandtl approach, Physica A: Statistical Mechanics and its Applications 527(2019) 121179.
[18] T. Hayat, A. Aziz, T. Muhammad, A. Alsaedi, Numerical simulation for Darcy-Forchheimer 3D rotating flow subject to binary chemical reaction and Arrhenius activation energy, Journal of Central South University 26(5)(2019) 1250–1259.
[19] T. Hayat, R. Rubina, A. Arsalan, A. Ahmed, Analysis of entropy generation for MHD flow of third grade nanofluid over a nonlinear stretching surface embedded in a porous medium, Physica Scripta 94(12)(2019) 125703.
[20] T. Hayat, A. Aziz, T. Muhammad, A. Alsaedi, Numerical simulation for three-dimensional flow of Carreau nanofluid over a nonlinear stretching surface with convective heat and mass conditions, Journal of the Brazilian Society of Mechanical Sciences and Engineering 41(1)(2019) 1–11.
[21] A. Hafeez, M. Khan, J. Ahmed, Stagnation point flow of radiative Oldroyd-B nanofluid over a rotating disk, Computer methods and programs in biomedicine 191(2020) 105342.
[22] Z. Shah, M. Sheikholeslami, P. Kumam, Simulation of entropy optimization and thermal behavior of nanofluid through the porous media, International Communications in Heat and Mass Transfer 120(2021) 105039.
[23] M. Sajid, T. Hayat, Influence of thermal radiation on the boundary layer flow due to an exponentially stretching sheet, International Communications in Heat and Mass Transfer 35(3)(2008) 347–56.
[24] B.J. Gireesha, G.M. Pavithra, C.S. Bagewadi, Boundary layer flow and heat transfer of a dusty fluid over an exponentially stretching sheet, British Journal of Mathematics & Computer Science 2(4)(2012) 187–97.
[25] A. Shafiq, Z. Hammouch, T.N. Sindhu, D. Baleanu, Statistical approach of mixed convective flow of third-grade fluid towards an exponentially stretching surface with

https://doi.org/10.58715/bangmodjmcs.2022.8.6

convective boundary condition, In Special Functions and Analysis of Differential Equations Chapman and Hall/CRC (2020) 307–319.
[26] S. Nadeem, M.N. Khan, N. Abbas, Transportation of slip effects on nanomaterial micropolar fluid flow over exponentially stretching, Alexandria Engineering Journal 59(5)(2020) 3443–50.
[27] C.Y. Cheng, Combined heat and mass transfer in natural convection flow from a vertical wavy surface in a power-law fluid saturated porous medium with thermal and mass stratification, International Communications in Heat and Mass Transfer 36(4)(2009) 351-356.
[28] O.K. Koriko, I.L. Animasaun, A.J. Omowaye, T. Oreyeni, The combined influence of nonlinear thermal radiation and thermal stratification on the dynamics of micropolar fluid along a vertical surface, Multidiscipline Modeling in Materials and Structures (2018).
[29] Y.S. Daniel, Z.A. Aziz, Z. Ismail, A. Bahar, F. Salah, Stratified electromagnetohydrodynamic flow of nanofluid supporting convective role, Korean Journal of Chemical Engineering 36(7)(2019) 1021–32.
[30] I. Tlili, S. Naseer, M. Ramzan, S. Kadry, Y. Nam, Effects of chemical species and nonlinear thermal radiation with 3D Maxwell nanofluid flow with double stratification-an analytical solution, Entropy, 22(4)(2020) 453.
[31] F.O. Mallawi, M. Bhuvaneswari, S. Sivasankaran, S. Eswaramoorthi, Impact of double-stratification on convective flow of a non-Newtonian liquid in a Riga plate with Cattaneo-Christov double-flux and thermal radiation, Ain Shams Engineering Journal 12(1)(2021) 969–81.
[32] M. Waqas, Z. Asghar, W.A. Khan, Thermo-solutal Robin conditions significance in thermally radiative nanofluid under stratification and magnetohydrodynamics. The European Physical Journal Special Topics (2021) 1–10.
[33] M.M. Bhatti, E.E. Michaelides, Study of Arrhenius activation energy on the thermo-bioconvection nanofluid flow over a Riga plate, Journal of Thermal Analysis and Calorimetry 143(3)(2021) 2029-2038.
[34] U. Farooq, H. Waqas, M.I. Khan, S.U. Khan, Y.M. Chu, S. Kadry, Thermally radioactive bioconvection flow of Carreau nanofluid with modified Cattaneo-Christov expressions and exponential space-based heat source, Alexandria Engineering Journal 60(3)(2021) 3073–3086.
[35] H. Waqas, M. Imran, T. Muhammad, S.M. Sait, R. Ellahi, Numerical investigation on bioconvection flow of Oldroyd-B nanofluid with nonlinear thermal radiation and motile microorganisms over rotating disk, Journal of Thermal Analysis and Calorimetry 145(2)(2021) 523-539.
[36] M. Awais, S.E. Awan, M.A. Raja, N. Parveen, W.U. Khan, M.Y. Malik, Y. He, Effects of variable transport properties on heat and mass transfer in MHD bioconvective nanofluid rheology with gyrotactic microorganisms: numerical approach, Coatings 11(2)(2021) 231.
[37] S.U. Khan, K. Al-Khaled, M.M. Bhatti, Bioconvection analysis for flow of Oldroyd-B nanofluid configured by a convectively heated surface with partial slip effects, Surfaces and Interfaces 23(2021) 100982.
[38] S.J. Liao, The proposed homotopy analysis method for the solution of nonlinear problems. Ph.D. Thesis, Shanghai Jiao Tong University, Shanghai, China, (1992).

https://doi.org/10.58715/bangmodjmcs.2022.8.6

[39] S.J. Liao, An explicit, totally analytic approximate solution for Blasius viscous flow problems, Int. J. Non-Linear Mech. 34(1999) 759–778.
[40] S. Liao, Beyond perturbation: Introduction to the homotopy analysis method, CRC press; Boca Raton, FL, USA., 2003.
[41] M. Irfan, M. Khan, W.A. Khan, M. Sajid, Thermal and solutal stratifications in flow of Oldroyd-B nanofluid with variable conductivity, Appl. Phys. A 124(2018) 674.
[42] I. Tlili, H. Waqas, A. Almaneea, S.U. Khan, M. Imran, Activation energy and second order slip in bioconvection of Oldroyd-B nanofluid over a stretching cylinder: A proposed mathematical model, Processes 7(2019) 914.
[43] N.S. Khan, A.H. Usman, A. Kaewkhao, P. Kumam, P. Thounthong, U.W. Humphries, Exploring the nanomechanical concepts of development through recent updates in magnetically guided system, Scientific Reports 11(1)(2021) 1–22.
[44] T. Hayat, M. Waqas, S.A. Shehzad, A. Alsaedi, Mixed convection flow of viscoelastic nanofluid by a cylinder with variable thermal conductivity and heat source/sink, International Journal of Numerical Methods for Heat & Fluid Flow (2016).
[45] T. Hayat, I. Ullah, T. Muhammad, A. Alsaedi, Magnetohydrodynamic (MHD) three-dimensional flow of second grade nanofluid by a convectively heated exponentially stretching surface, Journal of Molecular Liquids 220(2016) 1004-1012.
[46] T. Hayat, S.A. Shehzad, A. Alsaedi, M.S. Alhothuali, Three-dimensional flow of Oldroyd-B fluid over surface with convective boundary conditions, Applied mathematics and Mechanics 34(4)(2013) 489–500.
[47] T. Hayat, T. Muhammad, S.A. Shehzad, A. Alsaedi, Temperature and concentration stratification effects in mixed convection flow of an Oldroyd-B fluid with thermal radiation and chemical reaction, PloS one 10(6)(2015) e0127646.

https://doi.org/10.58715/bangmodjmcs.2022.8.6